bioRxiv preprint doi: https://doi.org/10.1101/126466; this version posted June 9, 2017. The copyright holder for this preprint (which was not certified by peer review) is the author/funder, who has granted bioRxiv a license to display the preprint in perpetuity. It is made available under aCC-BY 4.0 International license.

Title: Cell type boundaries organize plant development

Authors: Monica Pia Caggiano[1#], Xiulian Yu[1#], Neha Bhatia[1#], André Larsson[2], Hasthi Ram[1], Carolyn Ohno[1], Pia Sappl[1], Elliot M. Meyerowitz[3], Henrik Jönsson[2,4,5], Marcus G. Heisler[1,6 *]

Affiliations:

[1] European Molecular Biology Laboratory, Meyerhofstrasse 1, D-69117 Heidelberg, Germany

[2] Computational Biology and Biological Physics, Department of Astronomy and Theoretical Physics, Lund University, Sweden

[3] Division of Biology and Biological Engineering and Howard Hughes Medical Institute, 156-29, California Institute of Technology, Pasadena, CA 91125, USA.

[4] Sainsbury Laboratory, University of Cambridge, Cambridge, UK

[5] Department of Applied Mathematics and Theoretical Physics, University of Cambridge, UK

[6] School of Life and Environmental Sciences, University of Sydney, NSW, Australia

# - these authors contributed equally to this work

* - author for correspondence: Marcus G Heisler (marcus.heisler@sydney.edu.au)

Once sentence summary: Cell type boundaries regulate plant development

Abstract: In plants the dorsoventral boundary of leaves defines an axis of symmetry through the centre of the organ separating the top (dorsal) and bottom (ventral) tissues. Although the positioning of this boundary is critical for leaf morphogenesis, how the boundary is established and how it influences development remains unclear. Using live-imaging and perturbation experiments we show that leaf orientation, morphology and position are pre-patterned by HD-ZIPIII and KAN gene expression in the shoot, leading to a model in which dorsoventral genes coordinate to regulate plant development by localizing auxin response between their expression domains. However we also find that auxin levels feedback on dorsoventral patterning by spatially organizing HD-ZIPIII and KAN expression in the shoot periphery. By demonstrating that the regulation of these

bioRxiv preprint doi: https://doi.org/10.1101/126466; this version posted June 9, 2017. The copyright holder for this preprint (which was not certified by peer review) is the author/funder, who has granted bioRxiv a license to display the preprint in perpetuity. It is made available under aCC-BY 4.0 International license.

genes by auxin also governs their response to wounds, our results also provide a parsimonious explanation for the influence of wounds on leaf dorsoventrality.

Introduction

Lateral organ development in plants and animals typically involves several processes occurring in a coordinated manner. These include organ positioning, the specification of different cell types and organ morphogenesis. Spatial cues specifying these processes are usually provided by a molecular pre-pattern present in precursor tissues, or from inductive signals emanating from neighboring regions. Unlike animals however, plant organs such as leaves arise continuously in regular patterns around the shoot apical meristem (SAM). Nevertheless, certain features of leaves are relatively constant including the restriction of their formation to the meristem periphery and their flattened, dorsoventral (top-bottom) orientation with respect to the shoot apex. How are these fundamental features specified?

Since the 1950s wounding experiments involving the isolation of leaf primordia from the meristem have suggested the presence of an inductive signal from the meristem that promotes dorsal identity within leaf primordia at the time of organ initiation (Reinhardt et al., 2005; Sussex, 1951). A variant on this theme is the proposal that transient auxin depletion in the adaxial (adjacent to the shoot axis) tissues of leaf primordia promotes dorsal identity (Qi et al., 2014). In contrast, other studies suggest that dorsoventral pattering is pre-established, being directly derived from central-peripheral patterning of the shoot (Hagemann and Gleissberg, 1996; Husbands et al., 2009; Kerstetter et al., 2001). Supporting this proposal is the observation that transcription factors involved in both dorsal and ventral cell fate are expressed in the SAM in a central and peripheral manner respectively and that they control polar differentiation similarly in both contexts (Emery et al., 2003; McConnell et al., 2001; Yadav et al., 2013). However overall, the manner in which leaf dorsoventrality is first established in leaves remains unresolved (Kuhlemeier and Timmermans, 2016).

bioRxiv preprint doi: https://doi.org/10.1101/126466; this version posted June 9, 2017. The copyright holder for this preprint (which was not certified by peer review) is the author/funder, who has granted bioRxiv a license to display the preprint in perpetuity. It is made available under aCC-BY 4.0 International license.

To explain how leaf dorsoventrality regulates morphogenesis, Waites and Hudson (1995) took a cue from wing development in Drosophila (Diaz-Benjumea and Cohen, 1993) and proposed that tissues located along the boundary between dorsal and ventral leaf tissues act as organizers by producing mobile signals that pattern lamina growth (Waites and Hudson, 1995). So far, several genes have been identified that are expressed along this boundary including KLUH (Anastasiou et al., 2007) and the WOX family transcription WOX1, WOX2 and PRS (Haecker et al., 2004; Matsumoto and Okada, 2001; Nakata et al., 2012). The WOX genes in particular are required for proper lamina growth but are expressed only at the boundary region suggesting they may promote long-range patterning (Nakata et al., 2012). However although their ectopic expression can cause filamentous outgrowths at the leaf base, overall lamina growth is fairly normal (Nakata et al., 2012) suggesting that additional factors must direct patterning. The WOX genes are also known to regulate the expression of both dorsal and ventrally expressed transcription factors and miRNAs (Nakata et al., 2012; Zhang et al., 2014; Zhang et al., 2017) indicating that the WOX genes promote lamina growth at least in-part by maintaining the integrity of dorsal and ventral expression domains. Overall, this leaves the question of how dorsoventral boundaries actually regulate morphogenesis still unanswered.

Besides influencing leaf differentiation and shape, genes involved in leaf dorsoventrality influence leaf position. For instance, Arabidopsis plants mutant for the KANADI (KAN) genes develop leaves ectopically from the hypocotyl and leaf tissues (Izhaki and Bowman, 2007) while plants mutant for the Class III HD-ZIP (HD-ZIPIII) genes develop leaves from the center of the shoot (Emery et al., 2003). These observations indicate that the developmental mechanisms that specify leaf dorsoventrality may also be involved in organ positioning although how these processes relate is unclear.

In this study we investigate the origin of dorsoventral patterning in detail. We show that new organs are centered on a pre-patterned boundary region located between the expression domains of HD-ZIPIII and KAN genes and that both KAN and HD-ZIPIII genes act to repress organogenesis where they are expressed. This leads to a model in which dorsoventral genes control leaf morphogenesis and positioning by localizing auxin

bioRxiv preprint doi: https://doi.org/10.1101/126466; this version posted June 9, 2017. The copyright holder for this preprint (which was not certified by peer review) is the author/funder, who has granted bioRxiv a license to display the preprint in perpetuity. It is made available under aCC-BY 4.0 International license.

transcriptional response, which then polarizes cells non-cell autonomously (Bhatia et al., 2016). However, we also show that dynamic auxin levels play a central role in determining boundary position by spatially organizing HD-ZIPIII and KAN1 expression in the periphery. By demonstrating that the regulation of these genes by auxin also governs their response to wounds, our results also provide a parsimonious explanation for the influence of wounds on leaf dorsoventrality.

Results

Genes involved in leaf dorsoventrality pre-pattern organ formation in the shoot

Although the expression of genes involved in leaf dorsoventrality are known to be expressed in distinct domains within the shoot, how these domains relate spatially and temporally to sites of organ inception has not been investigated. To address this question we used confocal microscopy to monitor the expression of several genes involved in specifying leaf dorsoventrality in the shoot apical meristem (SAM) in combination with the auxin efflux carrier PIN-FORMED1 (PIN1) using functional fluorescent protein reporters. We found proteins involved in leaf dorsoventrality to be localized in non-overlapping concentric patterns with the dorsal Class III HD-ZIP protein REVOLUTA (REV) (Otsuga et al., 2001) being detected centrally, as marked by the expression of REVp::REV-2×YPet (REV-2×YPet), and the ventral protein KANADI1 (KAN1) (Kerstetter et al., 2001) expressed peripherally, as marked by the expression of KAN1p::KAN1-2×GFP (KAN1-2×GFP) (Figure 1, A to E). These concentric domains not only encircled the meristem but also extended contiguously around initiating leaves and floral bract. Imaging PIN1p::PIN1-CFP (PIN1-CFP) (Gordon et al., 2007a) together with these reporters revealed regions of high PIN1-CFP expression, marking positions of organ inception (Heisler et al., 2005; Reinhardt et al., 2003), to be centered on a narrow region located between the dorsal and ventral domains (Figure 1D-K). This arrangement was conserved with few cells altering their KAN1 expression status during organogenesis (Figure 1C arrowhead and Figure 2 A-F). Ventrally expressed MIR165/166 (Kidner and Martienssen, 2004; Merelo et al., 2016; Nogueira et al., 2007; Yao et al., 2009) also appeared active in the SAM periphery as marked by a *MIR166Ap::GFPER* reporter and

bioRxiv preprint doi: https://doi.org/10.1101/126466; this version posted June 9, 2017. The copyright holder for this preprint (which was not certified by peer review) is the author/funder, who has granted bioRxiv a license to display the preprint in perpetuity. It is made available under aCC-BY 4.0 International license.

MIR165/166 biosensor (Figure 3A-I), consistent with previous studies (Miyashima et al., 2013). Both KAN1-2×GFP and *MIR166Ap::GFPER* re-established their expression in the SAM periphery after organ outgrowth (Figure 1E and Figure 3C arrowheads). As members of the WOX family of transcription factors including WOX1 and PRS are expressed at dorsoventral boundaries (Nakata et al., 2012) we imaged functional translational fusions to both PRS (PRSp::PRS- 2×GFP) and WOX1 (WOX1p:: 2×GFP-WOX1) to examine their expression in the shoot relative to leaves. We found that although 2×GFP-WOX1 expression was limited to the margins and middle domain of leaves (Figure 4A and B) and absent in the inflorescence meristem (Figure 4C), in the vegetative shoot PRS-2×GFP expression extended from the leaf middle domain to surround the SAM in a region between the KAN1 and REV expression domains (Figure 4D-H). In the inflorescence meristem however, PRS-2×GFP expression was restricted to early cryptic bract primordia (Figure 4I and J). In contrast to all genes described so far, a FILp::dsRED-N7 marker was expressed in both abaxial and adaxial cells at inception, consistent with a previous study (Tameshige et al., 2013) (Figure 5). Overall these data reveal that in many respects although not all, dorsoventral patterning within young leaf primordia, including the middle region (Nakata et al., 2012), corresponds to and is contiguous with, the patterning of dorsoventral gene expression in the SAM.

The KAN and Class III HD-ZIP genes repress organ initiation where they are expressed

The finding that sites of organ inception marked by PIN1 are located between KAN1 and REV expression domains in the SAM suggest that both KAN1 and REV may act to repress organ inception where they are expressed. Supporting this proposal, leaves develop ectopically in *kan1 kan2 kan4* and *rev phb phv* mutants (Izhaki and Bowman, 2007). However it is possible that the HD-ZIPIII genes influence organ initiation only indirectly by promoting SAM formation during embryogenesis (Emery et al., 2003; Izhaki and Bowman, 2007). To distinguish between these possibilities we induced the expression of MIR165/166-resistant REVr-2×VENUS throughout the epidermis using a pOp6/LhGR two-component (Samalova et al., 2005) system with the ATML1 promoter (Sessions et al., 1999) driving LhGR and found that it caused an arrest of organ formation

bioRxiv preprint doi: https://doi.org/10.1101/126466; this version posted June 9, 2017. The copyright holder for this preprint (which was not certified by peer review) is the author/funder, who has granted bioRxiv a license to display the preprint in perpetuity. It is made available under aCC-BY 4.0 International license.

and repression of KAN1-2×GFP in both the vegetative and inflorescence meristems (Figure 6 A-E). Despite the lack of organs, stem growth for the inflorescence meristem continued without any obvious change to meristem size, indicating that the phenotype initially influenced organ initiation (inset in Figure 6E). Similar results were observed after induction of a short tandem target mimicry construct designed to repress MIR165/166 activity (Yan et al., 2012) (Figure 6F and G) or after epidermal induction of MIR165/166-resistant PHAVOLUTA (Figure 6H-J). Similarly, plants expressing KAN1 ectopically in the epidermis also stopped making new organs (Figure 6K and L) and the inflorescence meristem took on a dome shape before eventually arresting (Figure 6M). We conclude both the KAN and Class III HD-ZIP genes regulate organ positioning at least in part by repressing organ initiation where they are expressed.

Expression patterns of REV and KAN1 in the shoot regulate leaf positioning and morphogenesis

To test whether boundaries between KAN1 and Class III HD-ZIP expression in the SAM can play an instructive role in positioning new organs and determining their subsequent dorsoventrality, we induced KAN1-2×GFP expression ectopically at the center of the SAM using a pOp6/LhGR two-component (Samalova et al., 2005) system and the CLV3 promoter driving LhGR. After KAN1-2×GFP induction, most seedlings initiated several new leaves before their growth stopped. Confocal imaging of seedlings five days after stratification (DAS) on dexamethasone (DEX) induction medium revealed that new organs, marked by high levels of PIN1-CFP expression, formed ectopically at the perimeter of an enlarged and irregular central domain of induced KAN1-2×GFP expression, in which REV-2×YPet expression had been repressed (Figure 7A and B). Although ectopic KAN1-2×GFP was only detected within or bordering organs during their initiation, REV-2×YPet expression was often restricted during later developmental stages (Figure 7C-H) indicating that patterns of KAN1 gene expression within the SAM can influence subsequent organ development. In particular, we noted that the distal margins of developing leaf primordia always correlated with boundaries of REV expression within the epidermis, even when REV expression was abnormally restricted (arrow heads in Figure 7C-H; movie S1). Several classes of phenotype, including leaves

bioRxiv preprint doi: https://doi.org/10.1101/126466; this version posted June 9, 2017. The copyright holder for this preprint (which was not certified by peer review) is the author/funder, who has granted bioRxiv a license to display the preprint in perpetuity. It is made available under aCC-BY 4.0 International license.

with an inverted orientation, could be distinguished at maturity (Figure 7 I-T) that correlated with the patterns of REV-2×YPet expression observed during early development. These distinct morphological classes can be explained according to the configuration of the HD-ZIPIII-KAN boundaries at organ inception. Specifically, we infer that the number and orientation of boundaries within organ founder cells (as specified by high auxin levels) determines the configuration of later leaf marginal tissue (Figure 7P-S).

Maximal auxin response is localized to HD-ZIPIII and KAN boundaries

The influence of dorsoventral gene expression on organogenesis suggests that dorsoventral boundaries may function generally to localize auxin response. In support of this proposal it has been reported that in the inflorescence meristem the auxin transcriptional marker DR5 is only responsive to auxin in the shoot periphery (de Reuille et al., 2006). We examined DR5 expression (Liao et al., 2015) in the vegetative meristem by examining its expression both in the wild type and after 1-N-Naphthylphthalamic acid (NPA) treatment at 3 DAS. In mock treated seedlings we found DR5 to be expressed at the locations of incipient primordia and at the distal tip of existing leaf primordia (Figure 8A and B). In contrast, NPA treated seedlings expressed DR5 in a ring encircling the SAM prior to organ emergence and in the middle domain or dorsoventral boundary region of developing leaves (Figure 8C and D). Similar experiments with seedlings expressing the ratiometric R2D2 intracellular auxin reporter (Liao et al., 2015) revealed a generally broader distribution of auxin compared to the DR5 transcriptional response, especially after NPA treatment, where signal was not restricted to the meristem periphery or leaf tip (Figure 8E-H). These results indicate that like the inflorescence meristem, auxin transcriptional response outside the periphery of the vegetative meristem appears repressed. Since we also observed PRS expression localized to the meristem periphery (Figure 4D), we tested whether PRS as well as WOX1 are auxin inducible and found that both genes respond to auxin treatment within 12 and 15 hrs respectively although their response was restricted to the boundary region (Figure 8I-P). Measuring transcript levels using qPCR indicated that the auxin response for both genes occurs at the transcriptional level (Figure 8Q).

bioRxiv preprint doi: https://doi.org/10.1101/126466; this version posted June 9, 2017. The copyright holder for this preprint (which was not certified by peer review) is the author/funder, who has granted bioRxiv a license to display the preprint in perpetuity. It is made available under aCC-BY 4.0 International license.

These results not only reveal that general auxin response is maximized at the dorsoventral boundary but also, that genes already known to be expressed at the boundary are auxin responsive. Considering our results altogether and the finding that KAN1 represses PRS and WOX1 in ventral tissues (Nakata et al., 2012), we suggest a general scenario in which KAN and HD-ZIPIII genes repress auxin response where they are expressed, leaving a narrow domain of auxin responsive cells in between their expression domains.

The absence of HD-ZIPIII and KAN expression in boundary regions may mediate boundary function

So far, our results suggest a simple model in which organ formation is localized to boundary regions due to the local absence of KAN and HD-ZIPIII expression in boundary cells. We tested this proposal *in silico* by implementing a previous model for phyllotaxis (Jonsson et al., 2006; Smith et al., 2006), now supported experimentally (Bhatia et al., 2016), that incorporates the polarization of PIN1 towards cells with high intracellular auxin concentrations. By assuming that both KAN1 and REV repress auxin-induced transcription and by including a narrow region of cells located between the KAN1 and REV expression domains the model was able to self-organize the periodic formation of auxin maxima along the boundary as predicted, compared to a broader distribution of maxima when such boundaries are not included (Figure 9A-D; compare 9B to 8D).

Auxin organises HD-ZIPIII and KAN expression in the shoot periphery

So far, our results indicate that both HD-ZIPIII and KAN1 suppress auxin-induced gene expression where they are expressed. However this does not exclude the possibility that auxin may play a role in patterning HD-ZIPIII and KAN expression. Indeed, REV expression typically extends towards PIN1 polarity convergence patterns in the meristem periphery and disappears in axil regions where auxin is depleted, suggesting a direct or indirect role for auxin in promoting REV expression (Figure 1) (Heisler et al., 2005). In contrast, a recent study indicated that high auxin levels promote ventral cell fate (Qi et al., 2014). To investigate any potential regulation of REV and KAN expression by auxin we treated inflorescence meristems with NAA as well as NPA to prevent rapid auxin

bioRxiv preprint doi: https://doi.org/10.1101/126466; this version posted June 9, 2017. The copyright holder for this preprint (which was not certified by peer review) is the author/funder, who has granted bioRxiv a license to display the preprint in perpetuity. It is made available under aCC-BY 4.0 International license.

redistribution and examined the response of both REV and KAN1. We found that the region in between the REV and KAN1 domains narrowed due to a slight expansion of REV expression (Figure 10A and B). This was confirmed by following cells over time where we found that while more cells expressed REV, KAN expression appeared static (Figure 10C-H). We observed a similar but a comparatively faster response upon treatment with 2,4-D (Figure 10-Figure Supplement 1). Apart from changes in REV we noticed that over the course of 36 hours, KAN1 expression did not appear as expected in regions separating floral bracts from the meristem (Figure 10B). In vegetative meristems this was more obvious where contiguous REV expression often appeared between the meristem and developing leaves where KAN1 expression would normally be expressed (Figure 11A-H; Movie S2). These results indicate exogenous auxin promotes HD-ZIPIII expression and represses KAN expression in cells not already expressing KAN1.

To test whether REV or KAN1 expression depend on endogenous auxin for their patterns of expression we treated triple marker plants with the TIR1 antagonist auxinole (Hayashi et al., 2012) and found that after 18 hrs of treatment KAN expression had expanded slightly toward the meristem center (Figure 12A and B; Figure 12-Figure Supplement 1A-D). As auxinole competes with endogenous auxin for the TIR1 binding pocket, we attempted to reduce endogenous auxin signaling further by simultaneously treating the meristems with yucasin (Nishimura et al., 2014) and kyn (He et al., 2011) to block auxin synthesis. This combination of treatments led to an arrest of organogenesis and “pin” phenotype as well as a significant expansion and restriction of KAN1 and REV expression centrally, respectively (Figure 12C and D; Figure 12-Figure Supplement 1E-H Figure 12-Figure Supplement 2). KAN expression not only expanded into those cells originally located between the REV and KAN1 domains but also cells that had previously been expressing REV at high levels. However KAN1 expression remained excluded from the central most cells of the shoot and established floral bracts and leaf primordia, where REV expression still remained (Figure 12D; Figure 12-Figure Supplement 2). Extending the drug treatment time did not lead to a further change in expression. Monitoring the ratiometric auxin sensor R2D2 in response to a similar combined inhibitor treatment

bioRxiv preprint doi: https://doi.org/10.1101/126466; this version posted June 9, 2017. The copyright holder for this preprint (which was not certified by peer review) is the author/funder, who has granted bioRxiv a license to display the preprint in perpetuity. It is made available under aCC-BY 4.0 International license.

confirmed a strong decrease in overall intracellular auxin levels, including in the central meristem regions where REV was still expressed (Figure 12 E and F).

Overall these data indicate that directly or indirectly, dynamic changes in auxin levels play a central role in regulating dorsal and ventral identities in a way that contrasts with previous proposals (Qi et al., 2014). Auxin not only triggers HD-ZIPIII expression in the periphery but also maintains this expression at the expense of KAN1 until a leaf or flower primordium is established. However, auxin only promotes HD-ZIPIII and represses KAN1 in cells not already expressing KAN1, i.e. once KAN1 is expressed, it is maintained even if auxin levels increase. This suggests a scenario in which the boundary between HD-ZIPIII and KAN expression in the SAM only becomes anchored to the underlying cells when auxin levels are high, i.e. at organ inception, consistent with our imaging data.

Wounding induced KAN expression in an auxin dependent manner

Since auxin is required to maintain REV at the expense of KAN expression in the meristem periphery and wounding causes repolarization of PIN1 away from wound sites (Heisler et al., 2010) resulting in auxin depletion (Landrein et al., 2015), we investigated whether wounding results in ectopic KAN1 and reductions in REV expression. Firstly, using a pulsed IR laser to ablate cells adjacent to young organ primordia we confirmed that auxin levels decrease in the vicinity of wounds by monitoring the expression of the R2D2 ratiometric marker (Figure 13A and B). Next, we monitored REV, KAN and PIN1 expression in response to such wounds. We found that KAN1 became expressed in cells adjacent to the wound on either side, regardless of wound orientation with respect to the SAM (Figure 13C and D; Figure 13-Figure Supplement 1A-H). Such a response argues against the possibility that ectopic KAN is the result of interruption of a signal emanating from the meristem that promotes dorsal and represses ventral identity (Sussex, 1955). Instead, it supports the proposal that KAN1 expression is promoted in the vicinity of wounds in general, possibly due to low auxin levels. To test this hypothesis, we repeated these experiments while treating the wounded meristems with combinations of NAA and NPA over a 48 hr period and found that the induction of KAN1 expression around

bioRxiv preprint doi: https://doi.org/10.1101/126466; this version posted June 9, 2017. The copyright holder for this preprint (which was not certified by peer review) is the author/funder, who has granted bioRxiv a license to display the preprint in perpetuity. It is made available under aCC-BY 4.0 International license.

304 wounds could be completely eliminated if NAA and NPA were combined (Figure 13E-G;
305 Figure 13-Figure Supplement 1I-L). Although a similar response to wounding was found
306 to occur in vegetative meristems, the wound response typically involved a more
307 substantial reorganization of meristem structure, possibly due to the small size of the
308 vegetative meristem relative to the wounds (Figure 13-Figure Supplement 1 M-O). When
309 new leaves subsequently formed, they were properly oriented with respect to the new
310 meristem organization.
311
312 **Discussion**
313 In this study we shed new light on a long-standing question regarding leaf dorsoventrality
314 in plants – when and how is it established? The early work of Sussex, based on
315 histological analysis and wounding experiments, suggested that initiating leaf primordia
316 require an inductive signal from meristem tissues to specify dorsal cell fate (Sussex,
317 1955). This proposal has been further supported by a more recent study in tomato
318 (Reinhardt et al., 2005). In contrast, other workers in the field have claimed that
319 dorsoventrality arises directly from radial patterning of the shoot (Hagemann and
320 Gleissberg, 1996) and that wounds may disrupt pre-existing polarity (Snow and Snow,
321 1959). Our results reveal that organs are pre-patterned by domains of KAN and HD-
322 ZIPIII expression in the shoot. The effect of ectopic KAN1 expression at the center of the
323 shoot on subsequent leaf positioning and growth is particularly striking and indicates that
324 the spatial arrangement of HD-ZIPIII and KAN expression present within organ founder
325 cells is incorporated into organs as they initiate and directs patterns of morphogenesis
326 (Figure 7P-S; Figure 14). However, the exact configuration of this pre-pattern, including
327 its propagation into developing organs, is dynamic and depends on changing auxin levels.
328 While high auxin levels promote HD-ZIPIII and represses KAN this is only true for cells
329 not already expressing KAN. Hence, at sites of incipient organ formation, where auxin is
330 concentrated in between the two expression domains, HD-ZIPIII expression is promoted
331 and maintained in cells adaxial to KAN expression as these cells divide and become
332 displaced peripherally. At the same time, this high auxin also prevents KAN expression
333 from expanding into HD-ZIPIII expressing cells, causing the boundary to remain
334 relatively static with respect to the underlying cells (Figure 14 A). However if auxin

bioRxiv preprint doi: https://doi.org/10.1101/126466; this version posted June 9, 2017. The copyright holder for this preprint (which was not certified by peer review) is the author/funder, who has granted bioRxiv a license to display the preprint in perpetuity. It is made available under aCC-BY 4.0 International license.

levels drop, for instance when PIN1 reverses polarity away from a primordium in adaxial cells (Heisler et al., 2005; Qi et al., 2014), HD-ZIPIII expression decreases and KAN expression takes its place (Figure 14B and C). Hence auxin "locks-in" the spatial arrangement of HD-ZIPIII and KAN expression within organ founder cells at organ inception until a later stage when the pattern becomes auxin independent. Elsewhere however, the pattern is dynamic.

Overall these results imply that the dorsoventral pattering of organs results from a four-step process: (i) signals during embryonic development establish concentric patterns of Class III HD-ZIP and KAN gene expression; (ii) the boundary between these domains helps to define sites for auxin-dependent organogenesis i.e. the meristem peripheral zone; (iii) As organs form, dynamic auxin levels modulate the patterns of HD-ZIPIII and KAN expression, thereby helping to position new organs and establish their dorsoventrality; (iv) patterns of HD-ZIPIII and KAN gene expression within organs are stabilized and dictate future patterns of morphogenesis.

The regulation of HD-ZIPIII and KAN expression by auxin is not only relevant to understanding wild type organ development but also for understanding the reorganization of tissue types in response to wounds. Wounds in the meristem outer cell layer specifically alter cell polarities such that PIN1 becomes polarized away from wounds in adjacent cells (Heisler et al., 2010), leading to auxin depletion (Landrein et al., 2015). As mentioned above, since the 1950s wounding has also been associated with changes in leaf dorsoventrality (Sussex, 1955). Specifically, wounds located between the meristem and initiating organ were found to promote leaf ventralization and a loss of lamina shape suggesting that the establishment of dorsal cell fate requires an inductive signal from the meristem, which the wound interrupted (Sussex, 1955). Our observations now indicate rather, that during organ establishment, HD-ZIPIII expression depends on high levels of auxin, which wounding disrupts. Thus as suggested previously, the meristem "acts by maintaining in the leaf-forming zone some polarized micro-structure which collapses without it" (Snow, 1959).

bioRxiv preprint doi: https://doi.org/10.1101/126466; this version posted June 9, 2017. The copyright holder for this preprint (which was not certified by peer review) is the author/funder, who has granted bioRxiv a license to display the preprint in perpetuity. It is made available under aCC-BY 4.0 International license.

The conclusions stated above contrast with those of another study reporting that high levels of auxin inhibit dorsal fate and promote ventral cell fate (Qi et al., 2014). These findings were based on auxin application experiments in tomato that resulted in the ventralization of leaves as well as the observation that Arabidopsis *pin1* and *pid rev* double mutants produce trumpet or rod-shaped shaped leaves. Although our results cannot easily explain the tomato data, since high auxin levels are required to maintain REV expression during organ establishment, we would expect that in *pin* and *pid* mutants, lower auxin levels may well result in lower expression levels of REV and possibly other Class III HD-ZIPs, leading to leaf ventralization as reported in these mutant backgrounds (Qi et al., 2014). Further auxin application experiments in tomato that include an analysis of gene expression and auxin level changes may clarify the relationship between auxin and dorsoventral patterning in tomato compared to Arabidopsis.

How do DV boundaries control organ position and shape? Both our data as well as data from previous studies suggest this is through the regulation of auxin perception. For instance, organ initiation requires high auxin levels but auxin can only trigger organogenesis in the peripheral zone (Reinhardt et al., 2000) where the HD-ZIPIII/KAN boundary occurs. A similar relationship holds for leaves where auxin application results in growth but only from the leaf margins, again corresponding to a DV boundary (Koenig et al., 2009). We further show that the localization of auxin response to DV boundaries applies generally, i.e. DR5 expression appears higher at such boundaries compared to the broader predicted auxin distribution, as marked by R2D2. How is this restriction achieved? Imaging data reveals that the locations of PIN1 polarity convergences correspond to a region of cells in between the expression domains of HD-ZIPIII and KAN where their expression is low or absent. Given our results as well as genetic and molecular data indicating that both the HD-ZIPIII and KAN genes repress auxin activity (Huang et al., 2014; Merelo et al., 2013; Zhang et al., 2017), we propose that this localized absence of expression results in a local de-repression of auxin-induced transcription. Such localized auxin activity has recently been shown to orient cell polarity,

bioRxiv preprint doi: https://doi.org/10.1101/126466; this version posted June 9, 2017. The copyright holder for this preprint (which was not certified by peer review) is the author/funder, who has granted bioRxiv a license to display the preprint in perpetuity. It is made available under aCC-BY 4.0 International license.

including microtubule orientations, in a non-cell autonomous manner (Bhatia et al., 2016). Hence, we suggest that the proposed ability of dorsoventral boundaries to act as organizers analogous to those of the Drosophila wing (Diaz-Benjumea and Cohen, 1993; Waites and Hudson, 1995) rests in-part on their ability to orient cell polarity non-cell autonomously by localizing auxin activity (Figure 14D). The resulting growth may either occur in the periodic fashion along the boundary typical of phyllotaxis and complex leaves, or in a more continuous manner typical of simple leaves, depending on the strength of auxin transport or other modifications to the cell polarity feedback system (Bilsborough et al., 2011; Koenig et al., 2009). Investigating the dynamic consequences of directly juxtaposing REV and KAN expression should enable the testing of these hypotheses as well as lead to a better understanding of how auxin responsive boundary domains are first established.

Materials and Methods

Plant material

Plants were grown on soil at 22 °C in continuous light-conditions and cultivated either on soil or on GM medium (1 % sucrose, 1× Murashige and Skoog basal salt mixture, 0.05% MES 2-(MN-morpholino)-ethane sulfonic acid, 0.8 % Bacto Agar, 1 % MS vitamins, pH 5.7 with 1 M potassium hydroxide solution).

Construction of Transgenes

Multiply transgenic lines were generated by Agrobacterium-mediated transformation into stable transgenic lines or by genetic crossing. The *FILp::dsREDN7* and *PIN1p::PIN1-GFP* transgenes have been described elsewhere (*16*). *pREV::REV-2×VENUS* in the T-DNA vector *pMLBART* (Gleave, 1992) is a modification of *pREV::REV-VENUS* (Heisler et al., 2005) that contains a translational fusion to 2 tandem copies of the fluorescent protein VENUS (Nagai et al., 2002). *REVp::REV-2×Ypet* containing a C-terminal fusion to the 2× Ypet (Nguyen and Daugherty, 2005) in *pMOA36* T-DNA (Barrell and Conner, 2006) was transformed into a *PINp::PIN1-CFP* line (Gordon et al., 2007b). The *KAN1p::KAN1-2×GFP* transgene in pMOA34 T-DNA was created by amplifying 8.7 kb of *KAN1* (At5g16560) genomic sequences with primers KAN1g F and KAN1g R

bioRxiv preprint doi: https://doi.org/10.1101/126466; this version posted June 9, 2017. The copyright holder for this preprint (which was not certified by peer review) is the author/funder, who has granted bioRxiv a license to display the preprint in perpetuity. It is made available under aCC-BY 4.0 International license.

(Supplemental Data File 1A) as a translational fusion to a 9 Ala linker and 2×GFP followed by *OCS* terminator sequences. When transformed into *kan1-2 kan2-1* segregating plants, this construct complements the mutant phenotype. The triple marker line was generated by transforming *KAN1p::KAN1-2×GFP* into a *REVp::REV-2×Ypet; PIN1p::PIN1-CFP* transgenic line. *KAN1p::KAN1-2×CFP* or *KAN1p::KAN1-2×Ypet* containing a fusion to 2 copies of CFP or Ypet, respectively, were constructed similarly. *KAN1p::KAN1-2×Ypet* and *PIN1p::PIN1-GFP* were combined in T-DNA vector *BGW* (Karimi et al., 2002) by Gateway technology (Invitrogen) for generation of a double marker transgenic line.

The *KAN1* cDNA was amplified by PCR with primers K1 cDNA F and K1 cDNA R to generate C-terminal translational fusion to a 9 Ala linker followed by single GFP or 2×GFP followed by pea *rbcS E9* terminator sequence (Zuo et al., 2001) and cloned into the pOp6/LhGR two-component system (Craft et al., 2005) for dexamethasone-inducible misexpression.

An *ATML1p::LhGR* driver containing 3.4 kb of the L1-specific *ATML1* gene (At4g21750) fused to the chimeric LhGR transcription factor and a *6Op::KAN1-GFP* expression construct in a *pSULT* sulfadiazine-resistant T-DNA vector (*ATML1>>KAN1-GFP*) was generated. The *pSULT* T-DNA vector was derived from *pMLBART* by replacing the *NOSp::BAR* gene with *1'-2'p::*SUL (Rosso et al., 2003), a plant selectable marker that confers resistance to sulfadiazine herbicide to create *pSULT*. *A CLV3p::LhGR* driver containing 1.49 kb of upstream regulatory sequences was PCR amplified with primers CLV3p F and CLV3p R along with 1.35 kb of downstream regulatory sequences with primers CLV3utr F and CLV3utr R was combined with *6Op::KAN1-2×GFP* in *pSULT* T-DNA vector (*CLV3>>KAN1-2×GFP*).

ATML1>>REVr-2×VENUS is a sulfadiazine-resistant T-DNA vector to misexpress microRNA resistant REV-2×VENUS fusion, where *6Op::REVr-2×VENUS* was constructed by cloning a 1148 bp *Bam*HI-*Xcm*I microRNA resistant REV cDNA (a gift from J. Bowman) harbouring two previously characterized silent mutations that disrupt the binding of MIRNA 165/166 to the coding sequence of *REV* as previously described (Emery et al., 2003) downstream of the *6Op* and in frame with the wild type *REV-2×VENUS* coding sequences.

bioRxiv preprint doi: https://doi.org/10.1101/126466; this version posted June 9, 2017. The copyright holder for this preprint (which was not certified by peer review) is the author/funder, who has granted bioRxiv a license to display the preprint in perpetuity. It is made available under aCC-BY 4.0 International license.

453 *miR166Ap::GFPER* T-DNA construct was kindly provided by K. Nakajima (Miyashima
454 et al., 2011). The MIR165/166 biosensor was created based on the design presented by
455 Smith Z. R. et al. (Smith and Long, 2010) in the AlcR/AlcA expression system (Roslan et
456 al., 2001) for ethanol-inducible expression. The sequences conferring MIR165/166
457 sensitivity from the *REV* coding sequence (*REV*) and the sequences conferring
458 MIR165/166 insensitivity (REVr) were fused to *mCherry* (Shaner et al., 2004) with
459 endoplasmic reticulum localization sequences *mCherryER*, which was synthesized de
460 novo (Genscript). The MIR165/166-*mCherryER* biosensors (both biosensor and control)
461 were cloned as *Hind*III-*Bam*HI fragments downstream of the *AlcA* regulatory sequences
462 in the *UBQ10p:AlcR_BJ36* plasmid vector. *UBQ10p:AlcR* was constructed by cloning the
463 *UBQ10* promoter 2 kb fragment upstream of *AlcR* and the *OCS* terminator. Both
464 *UBQ10p::AlcR* and *AlcA::REV-mCherryER* or *AlcA::REVr-mCherryER* components
465 were combined in the T-DNA vector *pMOA34*.
466 The *WOX1p::2×GFP-WOX1* construct in *pMLBART* T-DNA vector was generated as
467 follows: 2.2 kb of *WOX1 (At3g18010)* upstream promoter sequence was amplified with
468 primers WOX1p F and WOX1p R and cloned using restriction enzymes KpnI and
469 BamHI. 3.6 kb of *WOX1* coding sequence plus 1.65 kb 3'-regulatory sequences was
470 amplified from wild-type Col-O genomic DNA with the primers WOX1g F and WOX1g
471 R and cloned using restriction enzymes *Bgl*II and *Spe*I. 2 copies of GFP were inserted in
472 frame at the start of the *WOX1* coding sequence at the *Bam*HI and *Bgl*II sites. A double
473 marker was generated by transforming the *WOX1p::2×GFP-WOX1* into *a PIN1p::PIN1-*
474 *C*FP transgenic line.
475 The *PRSp::PRS-2×GFP* construct in *pMOA34* T-DNA vector was made by amplification
476 of 3.9 kb *PRS (At2g28610)* genomic sequence (similar to (Shimizu et al., 2009)) with
477 primers PRSg F and PRSg R to create a C-terminal fusion to *2×GFP* followed by *OCS*
478 3'regulatory sequences. Marker combinations were generated by transforming the
479 *PRSp::PRS-2×GFP* into either a *PIN1p::PIN1-CFP* transgenic line or into *REVp::REV-*
480 *2×YPET PIN1p::PIN1-CFP* line. *(PRSp::PRS-2×GFP)* and *(KAN1p::KAN1-2×CFP)*
481 were combined in T-DNA vector BGW (Karimi et al., 2002) by Gateway technology
482 (Invitrogen) for generation of a double marker transgenic lines.

bioRxiv preprint doi: https://doi.org/10.1101/126466; this version posted June 9, 2017. The copyright holder for this preprint (which was not certified by peer review) is the author/funder, who has granted bioRxiv a license to display the preprint in perpetuity. It is made available under aCC-BY 4.0 International license.

A short tandem target mimic (STTM) construct to target MIR165/166 (Yan et al., 2012) was generated in the *pOp6/LhGR* two-component system for dexamethasone-inducible expression with a *UBQ10p::GRLh* driver. *STTM MIR165/166-88* sequence (Yan et al., 2012) was synthesized de novo (Genscript) and cloned downstream of *6×Op* to create *6×Op::STTM 165/166*. Both components were combined in a sulfadiazine T-DNA *pSULT* (*UBQ10>>STTM 165/166*).

ATML1>>PHVr is a sulfadiazine-resistant T-DNA vector containing a mutated version of *PHV* cDNA (a gift from J. Bowman) with a Gly to Asp amino acid change that disrupts the miRNA165/166 binding site in the *PHV* gene (McConnell et al., 2001). *6×Op::PHVr* was constructed by cloning a 2.6 kb *Xho*I-*Bam*HI *PHVr* cDNA downstream of *6×Op* and upstream of *pea3A* terminator sequences. *ATML1>>PHVr* was transformed into a *REVp::REV-2×YPet; PIN1p::PIN1-CFP* transgenic line.

DR5-3×VENUS v2 reporter gene (Liao et al., 2015) was a generous gift from D. Weijers. The line *R2D2 PIN1p::PIN1-GFP* was described previously (Bhatia et al., 2016).

Dexamethasone induction

For inducible gene perturbations in the vegetative SAM, seeds were germinated directly on GM medium containing 10 µM Dexamethasone (Sigma, stock solution was prepared in Ethanol).. Seedlings were then dissected for imaging at 4 DAS, 5 DAS or 7 DAS depending on the experiment. For DEX induction in the IM, 10 µM DEX solution containing 0.015% Silwet L-77 was applied to the IM every second day three times. Inflorescences were then dissected and imaged. The number of T2 inducible transgenic lines that exhibit the presented phenotypes and the frequencies of phenotypes amongst imaged plants is shown in Supplemental Data File 1B and associated caption.

Confocal Microscopy

Plants were dissected for imaging as previously described (Bhatia et al., 2016; Heisler and Ohno, 2014) and imaged with a Leica SP5 Upright confocal microscope using an Argon laser. The objective used was a water-immersion HCX IRAPO L25x/0.95 W (Leica). Excitation for CFP is 458 nm, GFP is 488 nm, YFP (Ypet and VENUS) is 514 nm and tdTomato is 561 nm. Emission signal were collected at 460-480 nm for CFP,

bioRxiv preprint doi: https://doi.org/10.1101/126466; this version posted June 9, 2017. The copyright holder for this preprint (which was not certified by peer review) is the author/funder, who has granted bioRxiv a license to display the preprint in perpetuity. It is made available under aCC-BY 4.0 International license.

490-512nm for GFP, 516-550 nm for YFP (YPet and VENUS), and 570-620 nm for tdTomato. The resulting z-stacks were processed using the Dye Separation (Channel mode or automatic mode) function available in the LAS AF program in order to separate the GFP channel from the YFP (Ypet or VENUS) channel. Three software packages: LAS AF from Leica, Imaris 8.0.2 by Bitplane and FIJI (https://fiji.sc) were used for data analysis. Ratios for R2D2 were calculated as described previously (Bhatia et al., 2016).

Measurement of distance between organs

For distance measurements between oppositely positioned leaves on plants transgenic for inducible KAN1 (*CLV3>>KAN1-2×GFP* – see above) the measurement tool from Imaris 8.0.2 (Bitplane) was used. For comparisons to control, untreated seedlings grown on GM were compared to seedlings grown on DEX for 5 days. t-Test was performed using Excel.

Chemical treatments for auxin depletion in the inflorescence meristems

500mM stock solutions of auxinole, yucasin and L-Kynurenine were prepared separately in DMSO. The stocks were diluted in 1mL 0.1M phosphate buffer in sterile water to make a working solution containing all the three drugs (0.2µL of each stock) to a final concentration of 100mM each. The final concentration of DMSO in the working solution containing all the three drugs was 0.06%.

Treatments were carried out on the inflorescence meristems of whole plants transplanted from soil to boxes containing GM medium supplemented with vitamins. The older flowers were removed as described (Heisler and Ohno, 2014). The plants were chosen such that the stem of the meristem was a few millimeters above the rosette to prevent the drug solution from dispersing into the surrounding medium. After imaging, the meristems were carefully dried using a thin strip of sterile filter paper to remove excess water. Approximately 50µL of the drug solution was added directly to the meristem, drop-wise. The meristems were treated only once in a time course of 12-18 hours.

NPA treatment on seedlings carrying R2D2 and DR5 markers

Seedling aged 3 DAS were dissected to expose the meristem and the first leaf pair as described (Bhatia et al., 2016). After imaging, seedlings were transferred to new GM

bioRxiv preprint doi: https://doi.org/10.1101/126466; this version posted June 9, 2017. The copyright holder for this preprint (which was not certified by peer review) is the author/funder, who has granted bioRxiv a license to display the preprint in perpetuity. It is made available under aCC-BY 4.0 International license.

medium containing plates and blotted dry with thin strips of sterile paper. 5-10µL of 100 µM NPA in sterile water (100 mM stock in DMSO) was added directly to the dissected seedlings every twenty-four hours for three days in total.

Auxin treatment on seedlings carrying PRS and WOX1 markers

Seedlings aged 4DAS (days after stratification) were dissected to expose the meristem and the first leaf pair as described (Bhatia et al., 2016). 5mM NAA (1M stock in 1M KOH) solution was prepared in liquid GM medium. Seedlings were then immersed in 100µL of NAA containing medium in individual wells in 96 well plate and grown under continuous light without shaking for 12 hours.

2-4,D treatment in the IMs expressing REV and KAN markers

For treatments with 2,4-D, the inflorescnce meristems were first imaged and then the treated with a few drops of 100 µM 2,4-D combined with 0.015% Silwet L-77. Apices were then imaged again 24 hrs later.

NAA, NPA and combined NAA and NPA treatments

For treatments on the vegetative meristems and the inflorescence, 3DAS old seedlings or the young inflorescences of plants expressing REV, KAN and PIN1 markers were dissected and imaged first. Samples were then treated with a combined solution of 100 µM NPA and 5mM NAA (both diluted in water) or 100 µM NPA alone or 5mM NAA alone. Samples were imaged and treated every 24hours for 72 hours in total.

Pulsed Laser ablations.

Laser ablations on the inflorescence meristems were carried out using the Mai Tai multi-photon laser from Spectra Physics, which was controlled with LEICA SP5 confocal software. Z-stacks were acquired prior to ablation. Single cells were targeted one after the other using bleach point mode. Ablations were carried out at 800nm with an output power of ~3W. Each pulse was shot for 1-15 milliseconds. Usually ablations were

bioRxiv preprint doi: https://doi.org/10.1101/126466; this version posted June 9, 2017. The copyright holder for this preprint (which was not certified by peer review) is the author/funder, who has granted bioRxiv a license to display the preprint in perpetuity. It is made available under aCC-BY 4.0 International license.

accomplished within 1-3 bursts of the laser. Ablated cells could be visually identified as their nuclei exploded resulting in unusual auto fluorescence. Z stacks were acquired immediately after the ablations.

Auxin and auxin plus NPA combined treatments on ablated inflorescence meristems

After ablations, the meristems were carefully blotted dry using thin strips of sterile filter paper. 20µL 5mM NAA in sterile water (0.5M stock in 1M KOH) or 20µL of a solution containing 5mM NAA and 100µM NPA in sterile water (100mM NPA stock in DMSO) or mock solution were added directly to the meristems every 24 hours for 48 hours in total.

Model for auxin and PIN1 dynamics

We developed a computational model to understand how interplay between the HD-ZIPIII and KAN pattern and PIN1 dynamics can influence auxin transport and primordia initiation. The model introduces a dependence on KANADI and REVOLUTA into previous models describing PIN1 and auxin dynamics (Bhatia et al., 2016; Heisler et al., 2010; Heisler and Jönsson, 2006; Jonsson et al., 2006; Sahlin et al., 2009). In the model, auxin resides in cell compartments and is able to move between cells either via active transport mediated by PIN1 proteins or passively via a diffusion-like process. PIN1 proteins cycle between cytosol and membrane compartments and a quasi-equilibrium model is used for determining its membrane localization at any time point. Auxin generates a signal able to polarise PIN1 in neighboring cells, i.e. a high auxin concentration increases the amount of PIN1 proteins in the neighboring cell membrane facing that cell. The molecule X in our model acts as a mediator of the signalling between auxin and PIN1, and the signal has previously been interpreted as a molecular (Jonsson et al., 2006), or mechanical stress signal (Heisler et al., 2010). In the model, the signal X is activated by auxin, and repressed by KAN and REV. The equations governing the dynamics of the molecules are

$$\frac{dA_i}{dt} = c_A - d_A A_i + \frac{1}{V_i}\left[D \sum_{j\in\{N_i\}} a_{ij}\left(A_j - A_i\right) + T \sum_{j\in\{N_i\}} a_{ij}\left(P_{ji}A_j - P_{ij}A_i\right)\right],$$

bioRxiv preprint doi: https://doi.org/10.1101/126466; this version posted June 9, 2017. The copyright holder for this preprint (which was not certified by peer review) is the author/funder, who has granted bioRxiv a license to display the preprint in perpetuity. It is made available under aCC-BY 4.0 International license.

$$\frac{dP_i^{[tot]}}{dt} = c_P - d_P P_i^{[tot]},$$

$$\frac{dX_i}{dt} = V_X \frac{A_i^{n_{XA}}}{(K_{XA}^{n_{XA}} + A_i^{n_{XA}})} \frac{K_{XR}^{n_{XR}}}{(K_{XR}^{n_{XR}} + R_i^{n_{XR}})} \frac{K_{XK}^{n_{XK}}}{(K_{XK}^{n_{XK}} + K_i^{n_{XK}})} - d_X X_i,$$

where A_i is the auxin concentration and X_i is the level of the signalling molecule in cell i. $\{N_i\}$ is the set of cells neighboring cell i, V_i is the cell volume of cell i, and $a_{ij} = a_{ji}$ is the cell wall area for the wall section between cells i and j. $P_i^{[tot]}$ is the total PIN1concentration in the cytosol and membrane compartments of cell i. Membrane-bound PIN1 appears in the equation as P_{ij}, which is the PIN1 concentration in the membrane compartment of cell i that faces cell j. A simple linear feedback between the signal X_j and P_{ij} is used and a quasi-stable assumption, introduced in Jönsson *et. al.* (2006), leads to

$$P_{ij} = \frac{P_i^{[tot]}[(1 - k_p) + k_p X_j]}{f_p + \sum_{k \in \{N_i\}}[(1 - k_p) + k_p X_k]},$$

where $f_p = k_n/k_x$ is the ratio of endocytosis and exocytosis rates and k_p sets the relation between symmetric and polarized exocytosis ($dP_{ij}/dt = k_x[(1-k_p) + k_p X_j]P_i - k_n P_{ij}$, where P_i is the PIN1 in the cytosol compartment). The feedback between auxin and PIN1 is identical to previous models if the KAN and REV factors in the dX_i/dt equation are 1 (e.g. by setting KAN and REV to zero in all cells), while the polarising signal becomes reduced in regions where KAN and/or REV are expressed. This effect tunes the interaction between the dorsoventral patterning and PIN1/auxin dynamics (cf. Figure. 8B and D).

The model was simulated using the in-house developed software organism/tissue (http://dev.thep.lu.se/organism/, available upon request). Files defining the model with parameter values (Supplemental Data File 1C) and initial configuration of (static) cell geometries and KAN and REV expression domains are provided as Supplemental Information. The simulations use a 5th order Runge-Kutta solver with adaptive step size

bioRxiv preprint doi: https://doi.org/10.1101/126466; this version posted June 9, 2017. The copyright holder for this preprint (which was not certified by peer review) is the author/funder, who has granted bioRxiv a license to display the preprint in perpetuity. It is made available under aCC-BY 4.0 International license.

(William H. Press, 2007), and initial auxin, PIN1 and X concentrations are set to zero in all compartments.

Generation of geometrical template

The model defined above was run on a template containing a predefined KAN/REV pattern (provided as Supplemental Data File 1C, Figure 9C). The geometry of the template was generated by a combination of cell/wall growth and mechanical interactions together with a shortest path division rule (Sahlin and Jonsson, 2010). A KAN/REV pattern was generated by the equations

$$\frac{dK_i}{dt} = V_K \frac{r_i^{n_K}}{K_K^{n_K} + r_i^{n_K}} - d_K K_i,$$

$$\frac{dR_i}{dt} = V_R \frac{r_i^{n_R}}{K_R^{n_R} + r_i^{n_R}} - d_R R_i.$$

This system was run to equilibrium on the above-mentioned template. In the above equations r_i is the distance of cell i from the center of the template. The parameters were set to V_K=V_R=d_K=d_R=1, K_K=30, K_R=25, n_K=n_R=20. These parameters are set such that two distinct domains are created, with a small overlap of low KAN and REV concentrations in the boundary between these regions. To make the transition of KAN concentrations between domains sharper, KAN concentrations were set to 0 (1) if $K_i \leqslant 0.5$ (>0.5).

Real time PCR

4 day-old wild-type Ler seedlings were immersed into 5mM NAA solution in liquid GM medium, and grown under continuous light without shaking for 15 hours. Cotyledons, hypocotyl, and roots were removed under dissecting scope, and only shoot meristem and the first pair of leaves were collected and immediately frozen in liquid nitrogen. Each biological replicate, represents tissue from 10-15 individual seedlings. Five biological replicates were collected for both mock and NAA treatment. RNeasy Mini kit (Qiagen) was used according to manufacturer's instruction for RNA extraction. 1 microgram of

bioRxiv preprint doi: https://doi.org/10.1101/126466; this version posted June 9, 2017. The copyright holder for this preprint (which was not certified by peer review) is the author/funder, who has granted bioRxiv a license to display the preprint in perpetuity. It is made available under aCC-BY 4.0 International license.

RNA was used for cDNA preparation using Super script III reverse transcriptase for Q-PCR analysis. Q-PCRs were performed in a StepOne Plus Real Time PCR system thermo cycler (The applied bio systems) using 20µl of PCR reaction containing 10 µL of SYBR Green mix (Roche), 1µl of primer mix (10µm), 2µl of 1:10 diluted cDNA and 7 µl of water. Transcript levels were normalized to ACTIN2 transcript levels. Data was analyzed using the $2^{-\Delta\Delta CT}$ method. A freely available online tool was used for analysis using an unpaired t-test of the RT-PCR results: http://graphpad.com/data-analysis-resource-center/. For p-value calculation, data entry format with mean, SD and N was used. Measurements and calculations for all replicates are provided in Source Data File for Figure 8.

Acknowledgements

We thank M. E. Byrne for helpful feedback and ideas on the manuscript. We thank J. Bowman for helpful discussions as well as for plasmids containing REVr and PHVr cDNAs. We thank D. Weijers and C. Y. Liao for a plasmid containing pDR5v2::ntdTomato; K. Nakajima for the T-DNA construct of miR166Ap::GFPER, Dr Atsushi Miyawaki from RIKEN Brain Science Institute for the VENUS fluorescent protein which was obtained through an MTA. The E.M.M. laboratory is supported by funds from the Howard Hughes Medical Institute and the Gordon and Betty Moore Foundation (through grant GBMF3406). The research leading to these results received funding from the Australian Research Council (M.G.H.) and European Research Council under the European Union's Seventh Framework Programme (FP/2007-2013) / ERC Grant Agreement n. 261081 (M.G.H.), as well as the People Programme (Marie Curie Actions) under REA grant agreement n. 255089 (P.S.). The work was also supported by: the European Molecular Biology Laboratory (X.Y., M.P.C., C.O., P.S, N.B., H.R. and M.G.H.); the EMBL International PhD Programme (X.Y., N.B. and M.P.C.); Gatsby Charitable Foundation (GAT3395/PR4) (H.J) and Swedish Research Council (VR2013-4632) (H.J). The authors declare no competing financial interests. Supplement contains additional data and movie. We declare there are no competing interests.

bioRxiv preprint doi: https://doi.org/10.1101/126466; this version posted June 9, 2017. The copyright holder for this preprint (which was not certified by peer review) is the author/funder, who has granted bioRxiv a license to display the preprint in perpetuity. It is made available under aCC-BY 4.0 International license.

680

681

682

683

684 **References**

685

686 **Anastasiou, E., Kenz, S., Gerstung, M., MacLean, D., Timmer, J., Fleck, C. and**
687 **Lenhard, M.** (2007). Control of plant organ size by KLUH/CYP78A5-dependent
688 intercellular signaling. *Dev Cell* **13**, 843-856.
689 **Barrell, P. J. and Conner, A. J.** (2006). Minimal T-DNA vectors suitable for
690 agricultural deployment of transgenic plants. *Biotechniques* **41**, 708-710.
691 **Bhatia, N., Bozorg, B., Larsson, A., Ohno, C., Jonsson, H. and Heisler, M. G.** (2016).
692 Auxin Acts through MONOPTEROS to Regulate Plant Cell Polarity and Pattern
693 Phyllotaxis. *Curr Biol* **26**, 3202-3208.
694 **Bilsborough, G. D., Runions, A., Barkoulas, M., Jenkins, H. W., Hasson, A.,**
695 **Galinha, C., Laufs, P., Hay, A., Prusinkiewicz, P. and Tsiantis, M.** (2011).
696 Model for the regulation of Arabidopsis thaliana leaf margin development. *Proc*
697 *Natl Acad Sci U S A* **108**, 3424-3429.
698 **Craft, J., Samalova, M., Baroux, C., Townley, H., Martinez, A., Jepson, I., Tsiantis,**
699 **M. and Moore, I.** (2005). New pOp/LhG4 vectors for stringent glucocorticoid-
700 dependent transgene expression in Arabidopsis. *Plant J.* **41**, 899-918.
701 **de Reuille, P. B., Bohn-Courseau, I., Ljung, K., Morin, H., Carraro, N., Godin, C.**
702 **and Traas, J.** (2006). Computer simulations reveal properties of the cell-cell
703 signaling network at the shoot apex in Arabidopsis. *Proc Natl Acad Sci U S A*
704 **103**, 1627-1632.
705 **Diaz-Benjumea, F. J. and Cohen, S. M.** (1993). Interaction between dorsal and ventral
706 cells in the imaginal disc directs wing development in Drosophila. *Cell* **75**, 741-
707 752.
708 **Emery, J. F., Floyd, S. K., Alvarez, J., Eshed, Y., Hawker, N. P., Izhaki, A., Baum,**
709 **S. F. and Bowman, J. L.** (2003). Radial patterning of Arabidopsis shoots by class
710 III HD-ZIP and KANADI genes. *Curr Biol* **13**, 1768-1774.
711 **Gleave, a. P.** (1992). A Versatile Binary Vector System with a T-DNA Organizational-
712 Structure Conducive to Efficient Integration of Cloned DNA into the Plant
713 Genome. *Plant Molecular Biology* **20**, 1203-1207.
714 **Gordon, S. P., Heisler, M. G., Reddy, G. V., Ohno, C., Das, P. and Meyerowitz, E.**
715 **M.** (2007a). Pattern formation during de novo assembly of the Arabidopsis shoot
716 meristem. *Development* **134**, 3539-3548.
717 **Gordon, S. P., Heisler, M. G., Reddy, G. V., Ohno, C., Das, P. and Meyerowitz, E.**
718 **M.** (2007b). Pattern formation during de novo assembly of the Arabidopsis shoot
719 meristem. *Development* **134**, 3539-3548.
720 **Haecker, A., Gross-Hardt, R., Geiges, B., Sarkar, A., Breuninger, H., Herrmann, M.**
721 **and Laux, T.** (2004). Expression dynamics of WOX genes mark cell fate

bioRxiv preprint doi: https://doi.org/10.1101/126466; this version posted June 9, 2017. The copyright holder for this preprint (which was not certified by peer review) is the author/funder, who has granted bioRxiv a license to display the preprint in perpetuity. It is made available under aCC-BY 4.0 International license.

722 decisions during early embryonic patterning in Arabidopsis thaliana. *Development*
723 **131**, 657-668.
724 **Hagemann, W. and Gleissberg, S.** (1996). Organogenetic capacity of leaves: The
725 significance of marginal blastozones in angiosperms. *Plant Syst. Evol.* **199**, 121-
726 152.
727 **Hayashi, K., Neve, J., Hirose, M., Kuboki, A., Shimada, Y., Kepinski, S. and Nozaki,**
728 **H.** (2012). Rational design of an auxin antagonist of the SCF(TIR1) auxin
729 receptor complex. *ACS chemical biology* **7**, 590-598.
730 **He, W., Brumos, J., Li, H., Ji, Y., Ke, M., Gong, X., Zeng, Q., Li, W., Zhang, X., An,**
731 **F., et al.** (2011). A small-molecule screen identifies L-kynurenine as a
732 competitive inhibitor of TAA1/TAR activity in ethylene-directed auxin
733 biosynthesis and root growth in Arabidopsis. *Plant Cell* **23**, 3944-3960.
734 **Heisler, M. G., Hamant, O., Krupinski, P., Uyttewaal, M., Ohno, C., Jonsson, H.,**
735 **Traas, J. and Meyerowitz, E. M.** (2010). Alignment between PIN1 polarity and
736 microtubule orientation in the shoot apical meristem reveals a tight coupling
737 between morphogenesis and auxin transport. *PLoS Biol* **8**, e1000516.
738 **Heisler, M. G. and Jönsson, H.** (2006). Modeling Auxin Transport and Plant
739 Development. *Journal of Plant Growth Regulation* **25**, 302-312.
740 **Heisler, M. G. and Ohno, C.** (2014). Live-imaging of the Arabidopsis inflorescence
741 meristem. In *Flower Development*, pp. 431-440: Springer.
742 **Heisler, M. G., Ohno, C., Das, P., Sieber, P., Reddy, G. V., Long, J. A. and**
743 **Meyerowitz, E. M.** (2005). Patterns of auxin transport and gene expression
744 during primordium development revealed by live imaging of the Arabidopsis
745 inflorescence meristem. *Current Biology* **15**, 1899-1911.
746 **Huang, T., Harrar, Y., Lin, C., Reinhart, B., Newell, N. R., Talavera-Rauh, F.,**
747 **Hokin, S. A., Barton, M. K. and Kerstetter, R. A.** (2014). Arabidopsis
748 KANADI1 acts as a transcriptional repressor by interacting with a specific cis-
749 element and regulates auxin biosynthesis, transport, and signaling in opposition to
750 HD-ZIPIII factors. *Plant Cell* **26**, 246-262.
751 **Husbands, A. Y., Chitwood, D. H., Plavskin, Y. and Timmermans, M. C.** (2009).
752 Signals and prepatterns: new insights into organ polarity in plants. *Genes Dev* **23**,
753 1986-1997.
754 **Izhaki, A. and Bowman, J. L.** (2007). KANADI and class III HD-Zip gene families
755 regulate embryo patterning and modulate auxin flow during embryogenesis in
756 Arabidopsis. *Plant Cell* **19**, 495-508.
757 **Jonsson, H., Heisler, M. G., Shapiro, B. E., Meyerowitz, E. M. and Mjolsness, E.**
758 (2006). An auxin-driven polarized transport model for phyllotaxis. *Proceedings of*
759 *the National Academy of Sciences of the United States of America* **103**, 1633-
760 1638.
761 **Karimi, M., Inze, D. and Depicker, A.** (2002). GATEWAY vectors for Agrobacterium-
762 mediated plant transformation. *Trends Plant Sci* **7**, 193-195.
763 **Kerstetter, R. A., Bollman, K., Taylor, R. A., Bomblies, K. and Poethig, R. S.** (2001).
764 KANADI regulates organ polarity in Arabidopsis. *Nature* **411**, 706-709.
765 **Kidner, C. A. and Martienssen, R. A.** (2004). Spatially restricted microRNA directs
766 leaf polarity through ARGONAUTE1. *Nature* **428**, 81-84.

bioRxiv preprint doi: https://doi.org/10.1101/126466; this version posted June 9, 2017. The copyright holder for this preprint (which was not certified by peer review) is the author/funder, who has granted bioRxiv a license to display the preprint in perpetuity. It is made available under aCC-BY 4.0 International license.

Koenig, D., Bayer, E., Kang, J., Kuhlemeier, C. and Sinha, N. (2009). Auxin patterns Solanum lycopersicum leaf morphogenesis. *Development* **136**, 2997-3006.

Kuhlemeier, C. and Timmermans, M. C. (2016). The Sussex signal: insights into leaf dorsiventrality. *Development* **143**, 3230-3237.

Landrein, B., Kiss, A., Sassi, M., Chauvet, A., Das, P., Cortizo, M., Laufs, P., Takeda, S., Aida, M., Traas, J., et al. (2015). Mechanical stress contributes to the expression of the STM homeobox gene in Arabidopsis shoot meristems. *eLife* **4**, e07811.

Liao, C. Y., Smet, W., Brunoud, G., Yoshida, S., Vernoux, T. and Weijers, D. (2015). Reporters for sensitive and quantitative measurement of auxin response. *Nat Methods* **12**, 207-210, 202 p following 210.

Matsumoto, N. and Okada, K. (2001). A homeobox gene, PRESSED FLOWER, regulates lateral axis-dependent development of Arabidopsis flowers. *Genes Dev* **15**, 3355-3364.

McConnell, J. R., Emery, J., Eshed, Y., Bao, N., Bowman, J. and Barton, M. K. (2001). Role of PHABULOSA and PHAVOLUTA in determining radial patterning in shoots. *Nature* **411**, 709-713.

Merelo, P., Ram, H., Pia Caggiano, M., Ohno, C., Ott, F., Straub, D., Graeff, M., Cho, S. K., Yang, S. W., Wenkel, S., et al. (2016). Regulation of MIR165/166 by class II and class III homeodomain leucine zipper proteins establishes leaf polarity. *Proc Natl Acad Sci U S A*.

Merelo, P., Xie, Y., Brand, L., Ott, F., Weigel, D., Bowman, J. L., Heisler, M. G. and Wenkel, S. (2013). Genome-wide identification of KANADI1 target genes. *PLoS One* **8**, e77341.

Miyashima, S., Honda, M., Hashimoto, K., Tatematsu, K., Hashimoto, T., Sato-Nara, K., Okada, K. and Nakajima, K. (2013). A comprehensive expression analysis of the Arabidopsis MICRORNA165/6 gene family during embryogenesis reveals a conserved role in meristem specification and a non-cell-autonomous function. *Plant Cell Physiol* **54**, 375-384.

Miyashima, S., Koi, S., Hashimoto, T. and Nakajima, K. (2011). Non-cell-autonomous microRNA165 acts in a dose-dependent manner to regulate multiple differentiation status in the Arabidopsis root. *Development* **138**, 2303-2313.

Nagai, T., Ibata, K., Park, E. S., Kubota, M., Mikoshiba, K. and Miyawaki, A. (2002). A variant of yellow fluorescent protein with fast and efficient maturation for cell-biological applications. *Nature Biotechnology* **20**, 87-90.

Nakata, M., Matsumoto, N., Tsugeki, R., Rikirsch, E., Laux, T. and Okada, K. (2012). Roles of the middle domain-specific WUSCHEL-RELATED HOMEOBOX genes in early development of leaves in Arabidopsis. *Plant Cell* **24**, 519-535.

Nguyen, A. W. and Daugherty, P. S. (2005). Evolutionary optimization of fluorescent proteins for intracellular FRET. *Nat Biotechnol* **23**, 355-360.

Nishimura, T., Hayashi, K., Suzuki, H., Gyohda, A., Takaoka, C., Sakaguchi, Y., Matsumoto, S., Kasahara, H., Sakai, T., Kato, J., et al. (2014). Yucasin is a potent inhibitor of YUCCA, a key enzyme in auxin biosynthesis. *Plant J* **77**, 352-366.

bioRxiv preprint doi: https://doi.org/10.1101/126466; this version posted June 9, 2017. The copyright holder for this preprint (which was not certified by peer review) is the author/funder, who has granted bioRxiv a license to display the preprint in perpetuity. It is made available under aCC-BY 4.0 International license.

Nogueira, F. T. S., Madi, S., Chitwood, D. H., Juarez, M. T. and Timmermans, M. C. P. (2007). Two small regulatory RNAs establish opposing fates of a developmental axis. *Genes & Development* **21**, 750-755.

Otsuga, D., DeGuzman, B., Prigge, M. J., Drews, G. N. and Clark, S. E. (2001). REVOLUTA regulates meristem initiation at lateral positions. *Plant J* **25**, 223-236.

Qi, J., Wang, Y., Yu, T., Cunha, A., Wu, B., Vernoux, T., Meyerowitz, E. and Jiao, Y. (2014). Auxin depletion from leaf primordia contributes to organ patterning. *Proc Natl Acad Sci U S A* **111**, 18769-18774.

Reinhardt, D., Frenz, M., Mandel, T. and Kuhlemeier, C. (2005). Microsurgical and laser ablation analysis of leaf positioning and dorsoventral patterning in tomato. *Development* **132**, 15-26.

Reinhardt, D., Mandel, T. and Kuhlemeier, C. (2000). Auxin regulates the initiation and radial position of plant lateral organs. *Plant Cell* **12**, 507-518.

Reinhardt, D., Pesce, E. R., Stieger, P., Mandel, T., Baltensperger, K., Bennett, M., Traas, J., Friml, J. and Kuhlemeier, C. (2003). Regulation of phyllotaxis by polar auxin transport. *Nature* **426**, 255-260.

Roslan, H. A., Salter, M. G., Wood, C. D., White, M. R., Croft, K. P., Robson, F., Coupland, G., Doonan, J., Laufs, P., Tomsett, A. B., et al. (2001). Characterization of the ethanol-inducible alc gene-expression system in Arabidopsis thaliana. *Plant J* **28**, 225-235.

Rosso, M. G., Li, Y., Strizhov, N., Reiss, B., Dekker, K. and Weisshaar, B. (2003). An Arabidopsis thaliana T-DNA mutagenized population (GABI-Kat) for flanking sequence tag-based reverse genetics. *Plant Mol Biol* **53**, 247-259.

Sahlin, P. and Jonsson, H. (2010). A modeling study on how cell division affects properties of epithelial tissues under isotropic growth. *PLoS One* **5**, e11750.

Sahlin, P., Soderberg, B. and Jonsson, H. (2009). Regulated transport as a mechanism for pattern generation: capabilities for phyllotaxis and beyond. *J Theor Biol* **258**, 60-70.

Samalova, M., Brzobohaty, B. and Moore, I. (2005). pOp6/LhGR: a stringently regulated and highly responsive dexamethasone-inducible gene expression system for tobacco. *Plant J.* **41**, 919-935.

Sessions, A., Weigel, D. and Yanofsky, M. F. (1999). The Arabidopsis thaliana MERISTEM LAYER 1 promoter specifies epidermal expression in meristems and young primordia. *Plant J* **20**, 259-263.

Shaner, N. C., Campbell, R. E., Steinbach, P. A., Giepmans, B. N., Palmer, A. E. and Tsien, R. Y. (2004). Improved monomeric red, orange and yellow fluorescent proteins derived from Discosoma sp. red fluorescent protein. *Nat Biotechnol* **22**, 1567-1572.

Shimizu, R., Ji, J., Kelsey, E., Ohtsu, K., Schnable, P. S. and Scanlon, M. J. (2009). Tissue specificity and evolution of meristematic WOX3 function. *Plant Physiol.* **149**, 841-850.

Smith, R. S., Guyomarc'h, S., Mandel, T., Reinhardt, D., Kuhlemeier, C. and Prusinkiewicz, P. (2006). A plausible model of phyllotaxis. *Proc Natl Acad Sci U S A* **103**, 1301-1306.

bioRxiv preprint doi: https://doi.org/10.1101/126466; this version posted June 9, 2017. The copyright holder for this preprint (which was not certified by peer review) is the author/funder, who has granted bioRxiv a license to display the preprint in perpetuity. It is made available under aCC-BY 4.0 International license.

Smith, Z. R. and Long, J. A. (2010). Control of Arabidopsis apical-basal embryo polarity by antagonistic transcription factors. *Nature* **464**, 423-426.

Snow, C. P. (1959). *The two cultures and the scientific revolution*. New York,: Cambridge University Press.

Snow, M. and Snow, R. (1959). The dorsiventrality of leaf primordia. *New Phytol* **58**, 19.

Sussex, I. M. (1951). Experiments on the cause of dorsiventrality in leaves. *Nature* **167**, 651-652.

Sussex, I. M. (1955). Morphogenesis in Solanum tuberosum I: experimental investigation of leaf dorsiventrality and orientation in the juvenile shoot. *Phytomorphology* **5**, 286-300.

Tameshige, T., Fujita, H., Watanabe, K., Toyokura, K., Kondo, M., Tatematsu, K., Matsumoto, N., Tsugeki, R., Kawaguchi, M., Nishimura, M., et al. (2013). Pattern dynamics in adaxial-abaxial specific gene expression are modulated by a plastid retrograde signal during Arabidopsis thaliana leaf development. *PLoS Genet* **9**, e1003655.

Waites, R. and Hudson, A. (1995). Phantastica - a Gene Required for Dorsoventrality of Leaves in Antirrhinum-Majus. *Development* **121**, 2143-2154.

William H. Press, S. A. T., William T. Vetterling, Brian P. Flannery (2007). *Numerical Recipes: The art of scientific computing* (3rd edn). New York, NY, USA: Cambridge University Press

Yadav, R. K., Perales, M., Gruel, J., Ohno, C., Heisler, M., Girke, T., Joensson, H. and Reddy, G. V. (2013). Plant stem cell maintenance involves direct transcriptional repression of differentiation program. *Molecular Systems Biology* **9**.

Yan, J., Gu, Y., Jia, X., Kang, W., Pan, S., Tang, X., Chen, X. and Tang, G. (2012). Effective small RNA destruction by the expression of a short tandem target mimic in Arabidopsis. *Plant Cell* **24**, 415-427.

Yao, X., Wang, H., Li, H., Yuan, Z., Li, F., Yang, L. and Huang, H. (2009). Two types of cis-acting elements control the abaxial epidermis-specific transcription of the MIR165a and MIR166a genes. *FEBS Lett* **583**, 3711-3717.

Zhang, F., Wang, Y., Li, G., Tang, Y., Kramer, E. M. and Tadege, M. (2014). STENOFOLIA recruits TOPLESS to repress ASYMMETRIC LEAVES2 at the leaf margin and promote leaf blade outgrowth in Medicago truncatula. *Plant Cell* **26**, 650-664.

Zhang, Z., Tucker, E., Hermann, M. and Laux, T. (2017). A Molecular Framework for the Embryonic Initiation of Shoot Meristem Stem Cells. *Dev Cell* **40**, 264-277 e264.

Zuo, J., Niu, Q. W., Moller, S. G. and Chua, N. H. (2001). Chemical-regulated, site-specific DNA excision in transgenic plants. *Nat Biotechnol* **19**, 157-161.

bioRxiv preprint doi: https://doi.org/10.1101/126466; this version posted June 9, 2017. The copyright holder for this preprint (which was not certified by peer review) is the author/funder, who has granted bioRxiv a license to display the preprint in perpetuity. It is made available under aCC-BY 4.0 International license.

901

bioRxiv preprint doi: https://doi.org/10.1101/126466; this version posted June 9, 2017. The copyright holder for this preprint (which was not certified by peer review) is the author/funder, who has granted bioRxiv a license to display the preprint in perpetuity. It is made available under aCC-BY 4.0 International license.

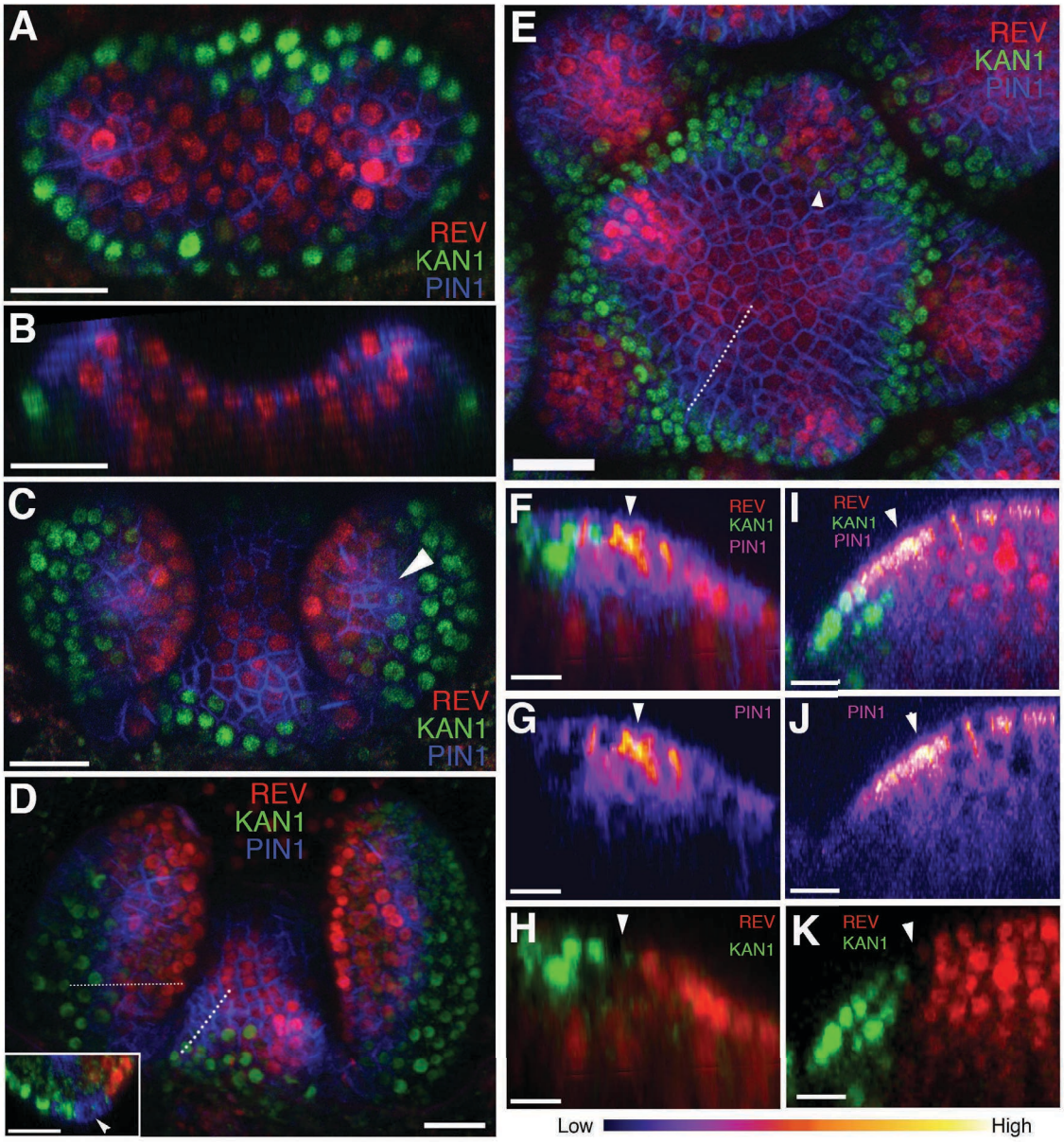

Figure 1.

Organ initiation is centered on a boundary between the expression domains of genes involved in leaf dorsoventrality.

(**A to D**) Confocal projections showing REV-2×YPet (red), PIN1-CFP (blue) and KAN1-2×GFP (green) expression in a vegetative shoot apical meristem at 3 days (A), 4 days (C) and 5 days (D) after stratification (DAS), respectively. Inset in (D) shows a transverse

bioRxiv preprint doi: https://doi.org/10.1101/126466; this version posted June 9, 2017. The copyright holder for this preprint (which was not certified by peer review) is the author/funder, who has granted bioRxiv a license to display the preprint in perpetuity. It is made available under aCC-BY 4.0 International license.

optical section across the dotted line in the left leaf. White arrowhead in the inset marks the cells in between the REV-2×YPet and KAN1-2×GFP expression domains where PIN1-CFP expression is highest. (**B**) Longitudinal reconstructed section of seedling shown in (A). (**E**) Expression pattern of REV-2×YPet, KAN1-2×GFP and PIN1-CFP in an inflorescence meristem. White arrow head marks region where KAN1-2×GFP expression is being reestablished after organ emergence. (**F to K**) Longitudinal optical sections across the dashed lines in (D) and (E) showing localized PIN1-CFP expression (magenta) marking organ inception at the REV-2×YPet /KAN1-2×GFP boundary in both the vegetative meristem (F-H) and inflorescence meristem (I-K). White arrow heads mark cells in between the REV-2×YPet and KAN1-2×GFP expression domains where PIN1-CFP expression is highest. Scale bars, 20 μm (A-E, inset in (D)) and 10 μm (F-K).

bioRxiv preprint doi: https://doi.org/10.1101/126466; this version posted June 9, 2017. The copyright holder for this preprint (which was not certified by peer review) is the author/funder, who has granted bioRxiv a license to display the preprint in perpetuity. It is made available under aCC-BY 4.0 International license.

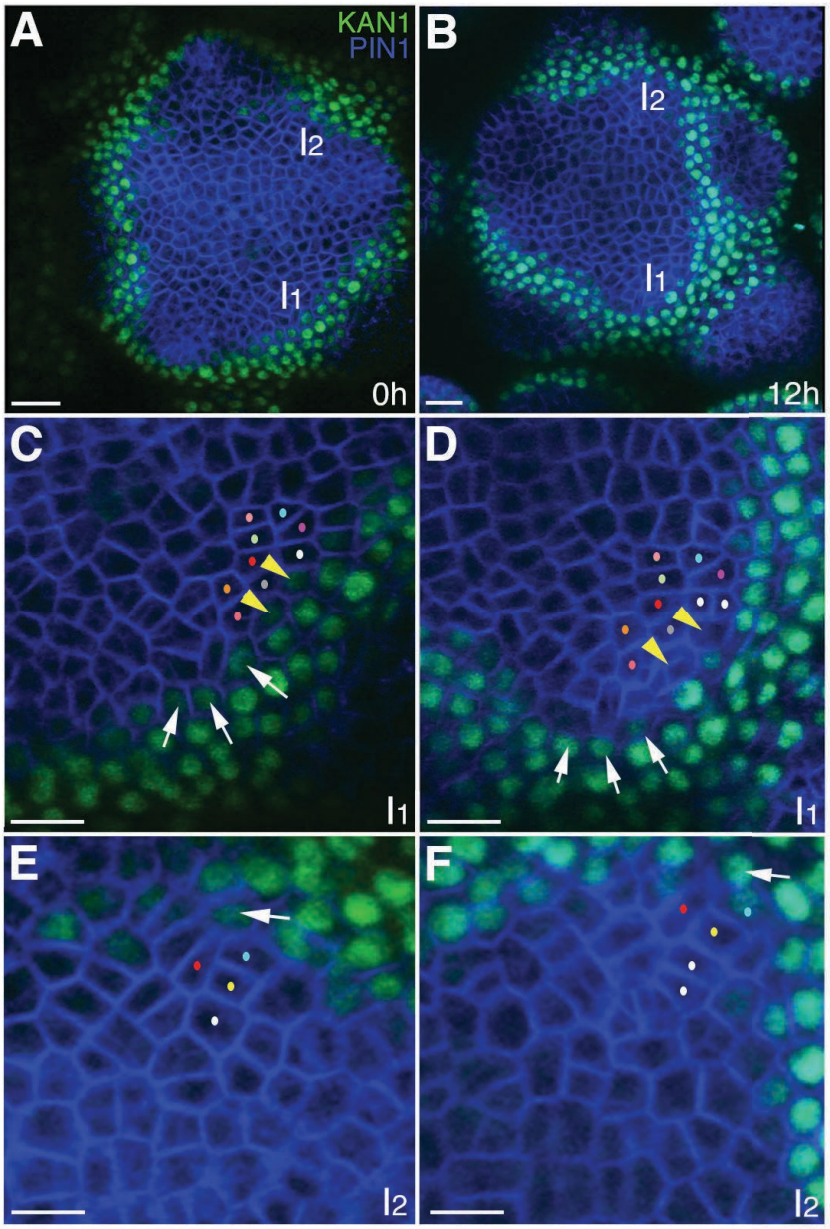

Figure 2.

The expression of KAN1-2×GFP is relatively stable with respect to the underlying cells within initiating organs.

(A-B) Confocal projections showing an inflorescence meristem viewed from above expressing PIN1-CFP (blue) and KAN1-2×GFP (green) at two time points (0h and 12h). Two incipient primordia are marked I1 and I2. **(C-D)** Close up views corresponding to primordium I1 from (A) and (B) with white arrows marking three cells at the edge of KAN1-2×GFP expression that retain this expression over the time interval. Yellow arrow

bioRxiv preprint doi: https://doi.org/10.1101/126466; this version posted June 9, 2017. The copyright holder for this preprint (which was not certified by peer review) is the author/funder, who has granted bioRxiv a license to display the preprint in perpetuity. It is made available under aCC-BY 4.0 International license.

933 heads mark two cells in which KAN1-2×GFP is absent at 12h. Similar colored dots mark
934 the same cells in (C) and (D), tracked over 12 hours. **(E)** Close up view of primordium I2
935 in (A) with arrow marking adaxial edge of KAN1 expression. (**F)** Close up of
936 primordium I2 in (B) showing the same cell marked in (E) remaining at the adaxial edge
937 of KAN1 expression after 12 hours. Similar colored dots mark the same cells in (E) and
938 (F), tracked over 12 hours. Scale bars, 20 μm in (A and B); 10 μm in (C-F).

939

bioRxiv preprint doi: https://doi.org/10.1101/126466; this version posted June 9, 2017. The copyright holder for this preprint (which was not certified by peer review) is the author/funder, who has granted bioRxiv a license to display the preprint in perpetuity. It is made available under aCC-BY 4.0 International license.

940

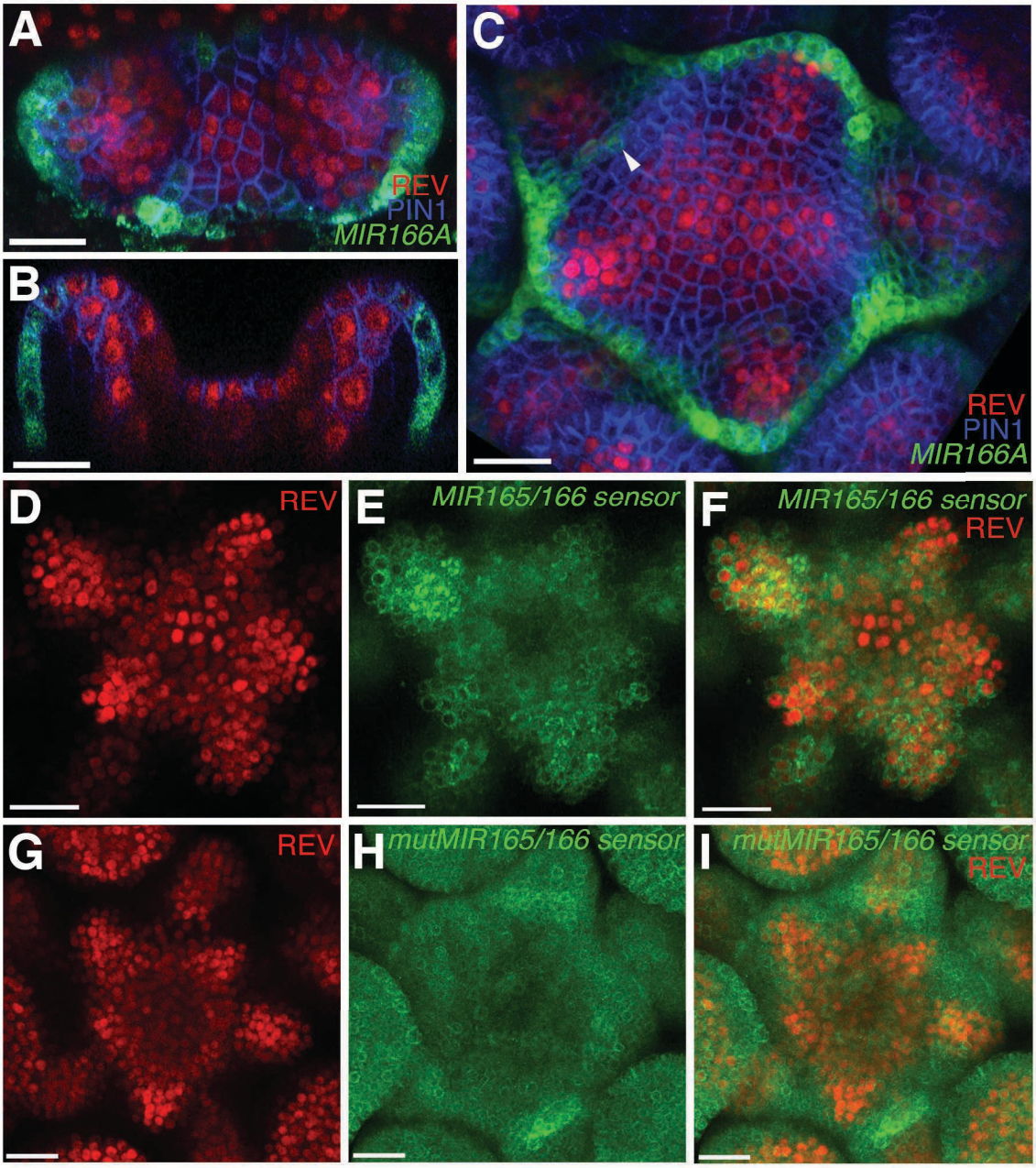

941

942 **Figure 3.**

943 **Expression and activity of MIR165/166 is localized to the periphery of the shoot**
944 **meristem.**

945 **(A)** Expression of *MIR166Ap::GFPER* (green), PIN1-CFP (blue) and REV-2×YPet (red)
946 in the vegetative meristem (VM) at 3.5 DAS. **(B)** Longitudinal section of meristem
947 shown in (A). **(C)** Expression of *MIR166Ap::GFPER* (green), PIN1-CFP (blue) and

bioRxiv preprint doi: https://doi.org/10.1101/126466; this version posted June 9, 2017. The copyright holder for this preprint (which was not certified by peer review) is the author/funder, who has granted bioRxiv a license to display the preprint in perpetuity. It is made available under aCC-BY 4.0 International license.

948 REV-2×YPet (red) in the inflorescence meristem (IM). White arrow head marks the
949 reestablishment of *MIR166Ap::GFPER* expression around the meristem after organ
950 emergence. **(D to F)** Expression of REV-2×YPet (red) alone (D), a MIR165/166
951 biosensor driven by the *UBQ10* promoter (green) alone (E) and both combined in the
952 same IM (F). (**G to I**) Corresponding control for (D to F) where the MIR165/166
953 biosensor has been rendered insensitive to MIRNA activity. Bars represent 20 μm.
954

bioRxiv preprint doi: https://doi.org/10.1101/126466; this version posted June 9, 2017. The copyright holder for this preprint (which was not certified by peer review) is the author/funder, who has granted bioRxiv a license to display the preprint in perpetuity. It is made available under aCC-BY 4.0 International license.

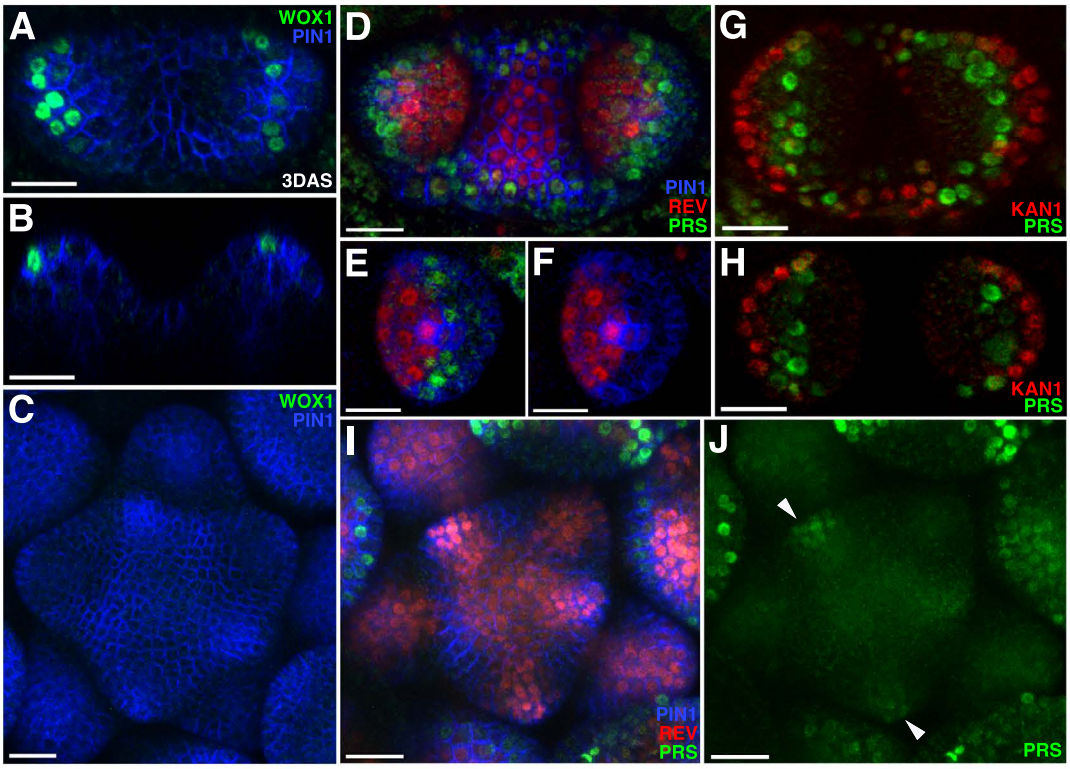

Figure 4.

Expression patterns of 2×GFP-WOX1 and PRS-2×GFP

Confocal projections showing PIN1-CFP (blue) and 2×GFP-WOX1 (green) expression patterns in the vegetative meristem and leaves of seedlings at 3 DAS. (**B**) Longitudinal section of meristem shown in (A). (**C**) An inflorescence meristem image showing 2×GFP-WOX1 is not expressed in the IM. (**D**) Confocal projection showing PIN1-CFP (blue), PRS-2×GFP (green) and REV-2×YPet (red) expression in the vegetative meristem and leaves at 3.5 DAS, where PRS-2×GFP is expressed surrounding the VM and along the leaf margins. (**E and F**) Cross sections of leaf on the right side in (D) showing the expression of PRS-2×GFP in the middle domain of the leaf. (**G and H**) Confocal projection and cross section showing PRS-2×GFP (green) and KAN1-2×CFP (red) expression patterns in the vegetative meristem and leaves of seedlings at 3 DAS. **(I and J)** PRS-2×GFP (green) is expressed in the young floral bracts in the IM, indicated with arrowhead in (J). Bar = 20 μm.

bioRxiv preprint doi: https://doi.org/10.1101/126466; this version posted June 9, 2017. The copyright holder for this preprint (which was not certified by peer review) is the author/funder, who has granted bioRxiv a license to display the preprint in perpetuity. It is made available under aCC-BY 4.0 International license.

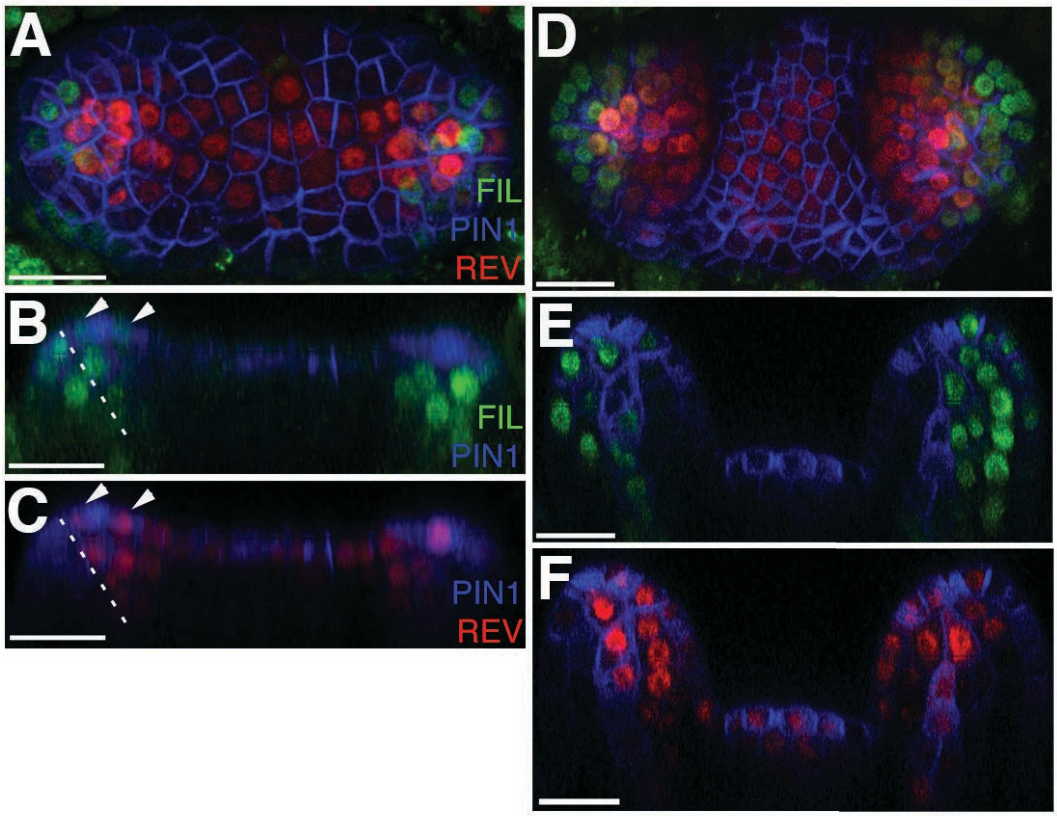

971

972 **Figure 5**

973 ***FILp::dsREDN7* expression is broad during leaf initiation but is later excluded from**
974 **dorsal tissues**. **(A-F)** Confocal projections and reconstructed sections of seedlings
975 expressing *FILp::dsREDN7* (green), REV-2×VENUS (red) and PIN1-CFP (blue). **(A)**
976 Top view of seedling at 3DAS **(B to C)** Longitudinal section of seedling shown in (A).
977 Dashed line shows dorsoventral axis of first leaf and arrowheads mark dorsal cells
978 expressing both REV-2×VENUS and *FILp::dsREDN7*. **(D)** Seedlings at 3.5 DAS with
979 *FILp::dsREDN7* expression more restricted to the developing ventral side of the leaf. **(E**
980 **to F)** Longitudinal sections of seedling shown in (D) showing a more complementary
981 pattern of *FILp::dsREDN7* relative to REV-2×VENUS compared to the earlier stage
982 shown in (A) to (C). Scale bars represent 20 μm.

983

984

bioRxiv preprint doi: https://doi.org/10.1101/126466; this version posted June 9, 2017. The copyright holder for this preprint (which was not certified by peer review) is the author/funder, who has granted bioRxiv a license to display the preprint in perpetuity. It is made available under aCC-BY 4.0 International license.

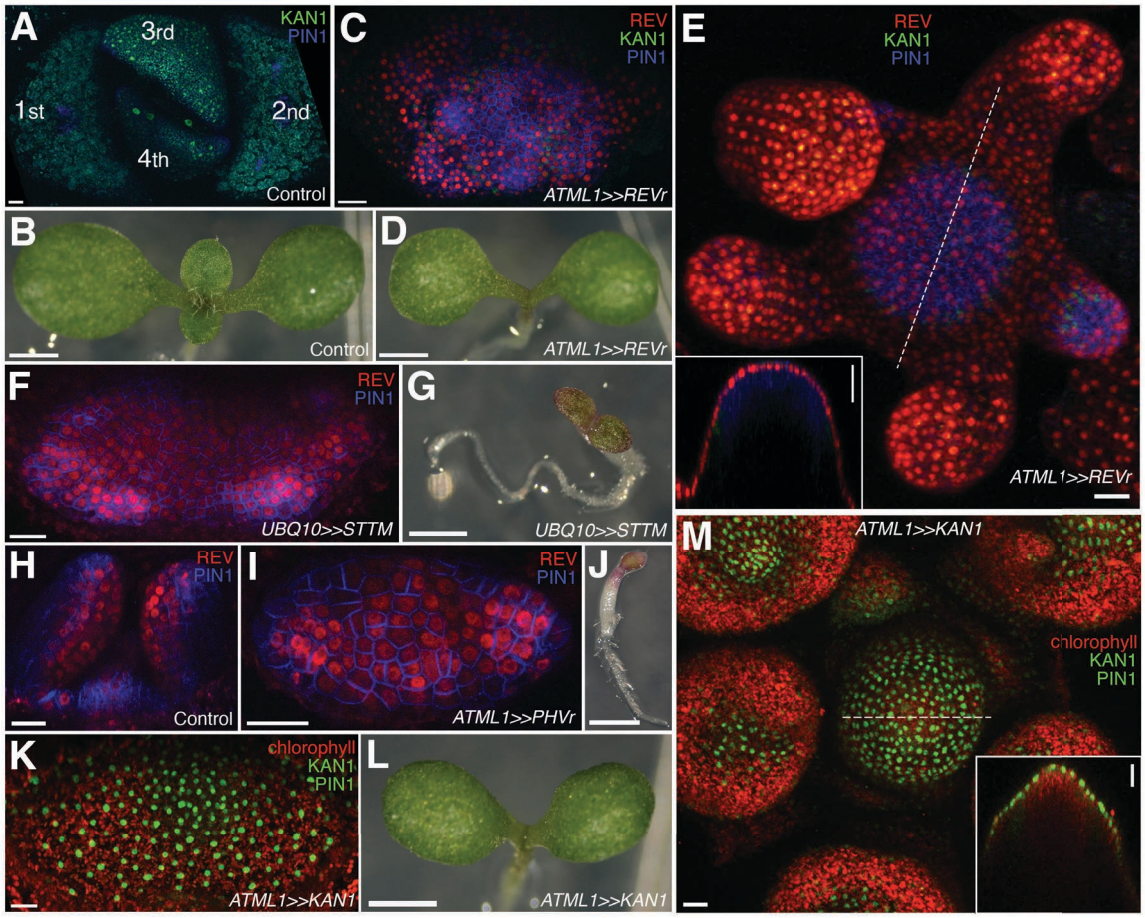

Figure 6.

Organ initiation depends on the restriction of Class III HD-ZIP and KANADI expression in the shoot.

(**A**) Confocal projection showing wild type control seedling at 7DAS viewed from above for comparison to (C) and (F). **(B)** Macroscopic view of control seedling at 7DAS for comparison to (D), (G) and (L). (**C**) Arrest of organogenesis after ectopic expression of REVr-2×VENUS from the *ATML1* promoter in the vegetative meristem (7 DAS) after germination on DEX, KAN1-2×GFP (green) expression is down regulated and could only be detected in a few cells in the sub-epidermis. Although PIN1-CFP (blue) expression is patchy, no leaves developed. **(D)** Macroscopic view of plant in (C). (**E**) Arrest of organogenesis after ectopic expression of REVr-2×VENUS (red) from the *ATML1* in the IM after 3 DEX treatments over 6 days. Note the absence of KAN1-2×GFP signal. Inset shows longitudinal optical section of the meristem across the dashed line. **(F)** Seedlings at 7DAS showing similar phenotype to (C) after induction of a short tandem target mimic

bioRxiv preprint doi: https://doi.org/10.1101/126466; this version posted June 9, 2017. The copyright holder for this preprint (which was not certified by peer review) is the author/funder, who has granted bioRxiv a license to display the preprint in perpetuity. It is made available under aCC-BY 4.0 International license.

(STTM) designed to down regulate MIR165/166 activity. **(G)** Macroscopic view of plant in (F). **(H to J)** Ectopic expression of REV-2YPet (red) and arrest of organogenesis (PIN1-CFP in blue) in 4DAS seedling after induction of MIR165/166 resistant PHAVOLUTA. (H) Longitudinal view of un-induced control. Top view (I), and macroscopic view (J) of induced seedling showing arrest of organ development. **(K and L)** Confocal projection (K) and macroscopic view (L) of seedling at 7DAS after induction of KAN1-GFP (green) in the epidermis. No leaves have developed (autofluorescence shown in red). (**M**) Arrest of organogenesis after induction of KAN1-GFP (green) driven by the *ATML1* promoter in the IM after 3 DEX treatments over 6 days; autofluorescence (red). Inset shows longitudinal optical section of the meristem across the dashed line. Scale bars represent 20 μm in (A, C, E, F, H to I, K and M); 1mm in (B, D, G, J and L).

bioRxiv preprint doi: https://doi.org/10.1101/126466; this version posted June 9, 2017. The copyright holder for this preprint (which was not certified by peer review) is the author/funder, who has granted bioRxiv a license to display the preprint in perpetuity. It is made available under aCC-BY 4.0 International license.

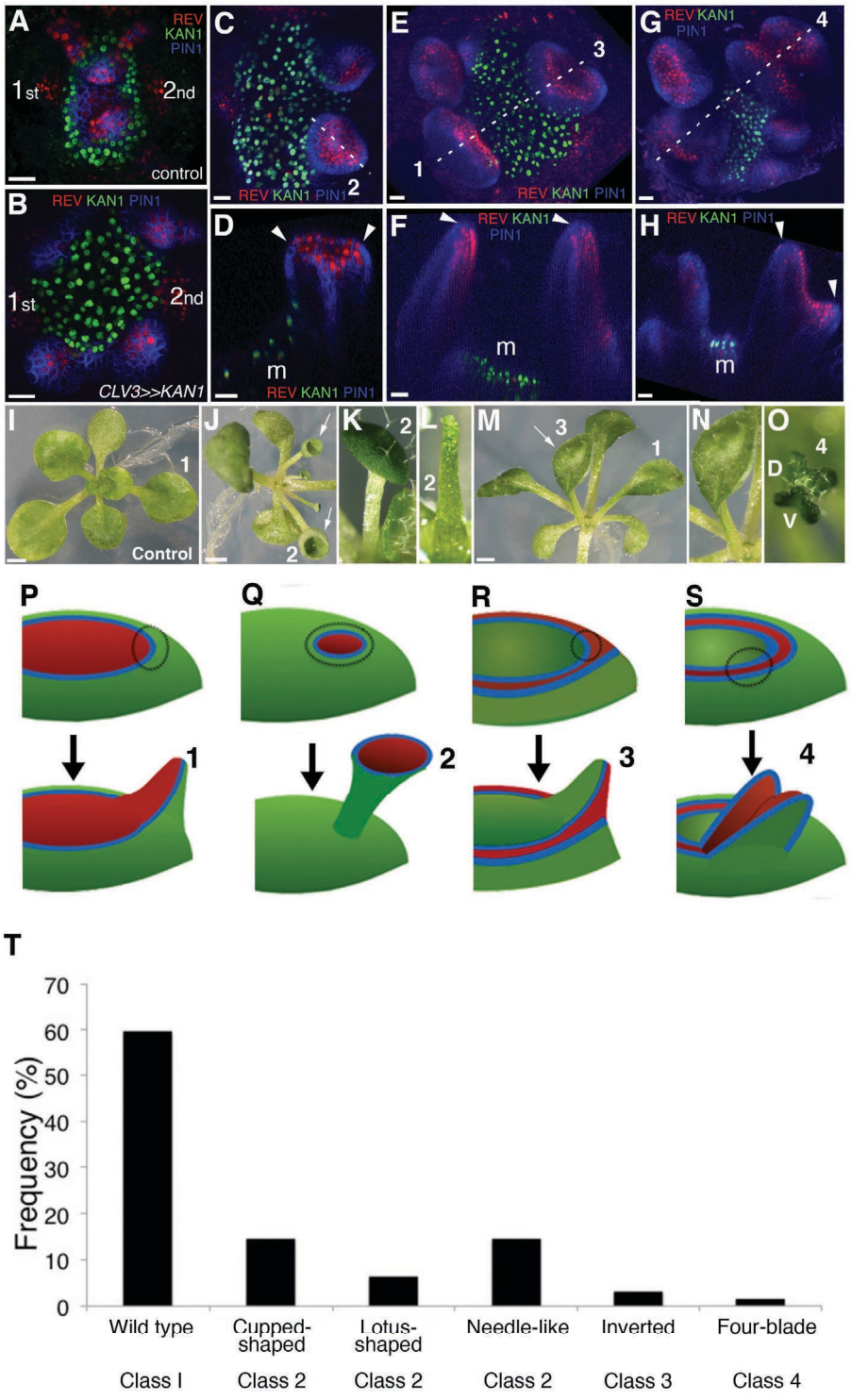

Figure 7.

KANADI1 expression boundaries in the shoot specify organ position and orientation.

bioRxiv preprint doi: https://doi.org/10.1101/126466; this version posted June 9, 2017. The copyright holder for this preprint (which was not certified by peer review) is the author/funder, who has granted bioRxiv a license to display the preprint in perpetuity. It is made available under aCC-BY 4.0 International license.

(**A and B**) Confocal projections showing organ initiation marked by REV-2×YPet (red) and PIN1-CFP (blue) at border of KAN1-2×GFP expression (green) in wild type (A) and after induction of KAN1-2×GFP using the *CLV3* promoter (B). Distance separating opposite organs was greater for induced (B) compared to control (A) (114.3 ±3.3 μm, n=19 vs 54.2±1.0 μm n=10 (mean±SE, $p<0.05$, t-test)). **(C to H)** Confocal projections (C, E and G) and longitudinal reconstructions corresponding to dashed lines (D, F and H respectively) showing restricted REV-2×YPet expression (red) after ectopic KAN1-2×GFP induction (green). Regions in which neither REV-2×YPet nor KAN1-2×GFP signal was detected may potentially express endogenous KAN1, which was not monitored. Four main configurations of REV expression and morphology were observed (labeled 1 to 4). Class 1 organs (E and F) correspond to the wild type, Class 2 (C and D) express REV-2×YPet centrally, Class 3 (E and F) express REV-2×YPet in a reversed orientation and Class 4 (G and H) express REV-2×YPet centrally and laterally only. Correspondence between REV-2×YPet expression boundaries and leaf margins indicated by arrowheads in D, F and H; m indicates meristem**.** Gamma value changed to highlight PIN1-CFP expression (blue) in (C) to (H). **(I to O)** Examples of mature leaves corresponding to Classes 1 to 4, including the WT (I), cup-shaped (J), lotus-shaped (a variation of cup-shaped) (K), needle-like (a further decrease in extent of dorsal tissue compare to cup-shaped) (L), inverted (M and N) and four bladed (O). "D and V" represent "dorsal" and "ventral" respectively in (O). **(P to S)** Diagrams summarizing proposed configurations of REV and KAN (green) gene expression in leaf founder cells (dashed circles) (upper diagram) leading to the observed phenotypic classes of leaf shape (numbered 1 to 4) (lower diagram) after induction of KAN1-2×GFP using the *CLV3* promoter. (P) represents the wild type Class 1 configuration, (Q) represents Class 2, (R) represents Class 3 and (S) represents Class 4. **(T)** Frequency of seedlings exhibiting different leaf morphologies after ectopic induction of KAN1-2×GFP expression in the CLV3 domain Class of phenotype corresponds to those indicated in (I to O). Scale bars = 20μm in A to H; 1 mm in I, J and M.

bioRxiv preprint doi: https://doi.org/10.1101/126466; this version posted June 9, 2017. The copyright holder for this preprint (which was not certified by peer review) is the author/funder, who has granted bioRxiv a license to display the preprint in perpetuity. It is made available under aCC-BY 4.0 International license.

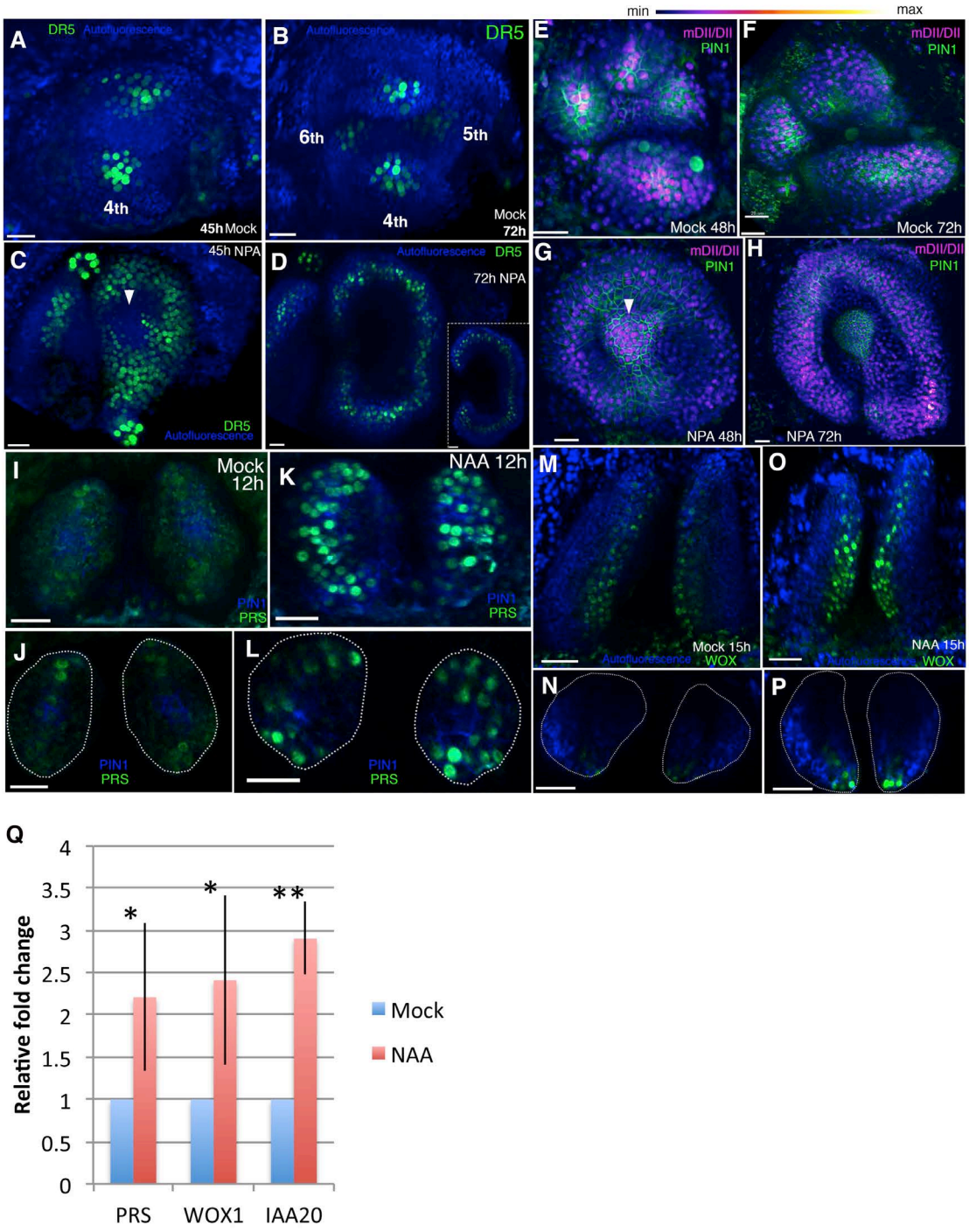

Figure 8.

Auxin promotes PRS and WOX expression.

(A-D) Response of pDR5V2-3×VENUS-N7 (green) auxin transcriptional reporter to NPA in Arabidopsis seedlings treated at 3DAS (Days after Stratification). (A and B)

bioRxiv preprint doi: https://doi.org/10.1101/126466; this version posted June 9, 2017. The copyright holder for this preprint (which was not certified by peer review) is the author/funder, who has granted bioRxiv a license to display the preprint in perpetuity. It is made available under aCC-BY 4.0 International license.

Confocal projections 45 hours (A) and 72 hours (B) after treatment with mock solution. (C and D) Confocal projections 45 hours (C) and 72 hours (D) after treatment with 100µM NPA solution (n=5/5). Inset in (D) shows transverse optical section through the ring-shaped organ showing most DR5 expression localized in the center of the organ. **(E-H)** Expression and response of R2D2 (magenta) to auxin along with PIN1-GFP expression (green) in Arabidopsis seedlings treated at 3DAS. (E and F) Confocal projections 48 hours (E) and 72 hours (F) after treatment with mock solution. (G and H) Confocal projections 48 hours (G) and 72 hours (H) after treatment with 100µM NPA solution (n=4/4). **(I-L)** Expression and response of pPRS:: PRS-2×GFP to auxin in Arabidopsis seedlings. Confocal projections and transverse optical slices of seedlings 4DAS showing of pPRS:: PRS-2×GFP expression (green) 12 hours after treatment with mock solution (I and J) and 5mM NAA (K and L) (n=5/5). **(M-P)** Expression and response of 2×GFP-WOX to auxin in Arabidopsis seedlings. (M and N) Confocal projections (M and O) and corresponding optical slices (N and P) of seedlings 4DAS showing pWOX1::2×GFP-WOX1 expression (green) 12 hours after treatment with mock solution (M and N) and 5mM NAA (O and P). Note WOX expression increases but does not expands beyond its regular expression domain upon auxin addition (n=5/5). **(Q)** Q-PCR analysis of PRS, WOX1 and positive control IAA20 transcripts after 5mM NAA or mock treatment on 4 days old wild-type (Ler) seedlings. *=$p<0.05$, **=$p<0.001$. Scale bars 20µm (A-L, K); 15µm (J and L); 30µm (M-P).

bioRxiv preprint doi: https://doi.org/10.1101/126466; this version posted June 9, 2017. The copyright holder for this preprint (which was not certified by peer review) is the author/funder, who has granted bioRxiv a license to display the preprint in perpetuity. It is made available under aCC-BY 4.0 International license.

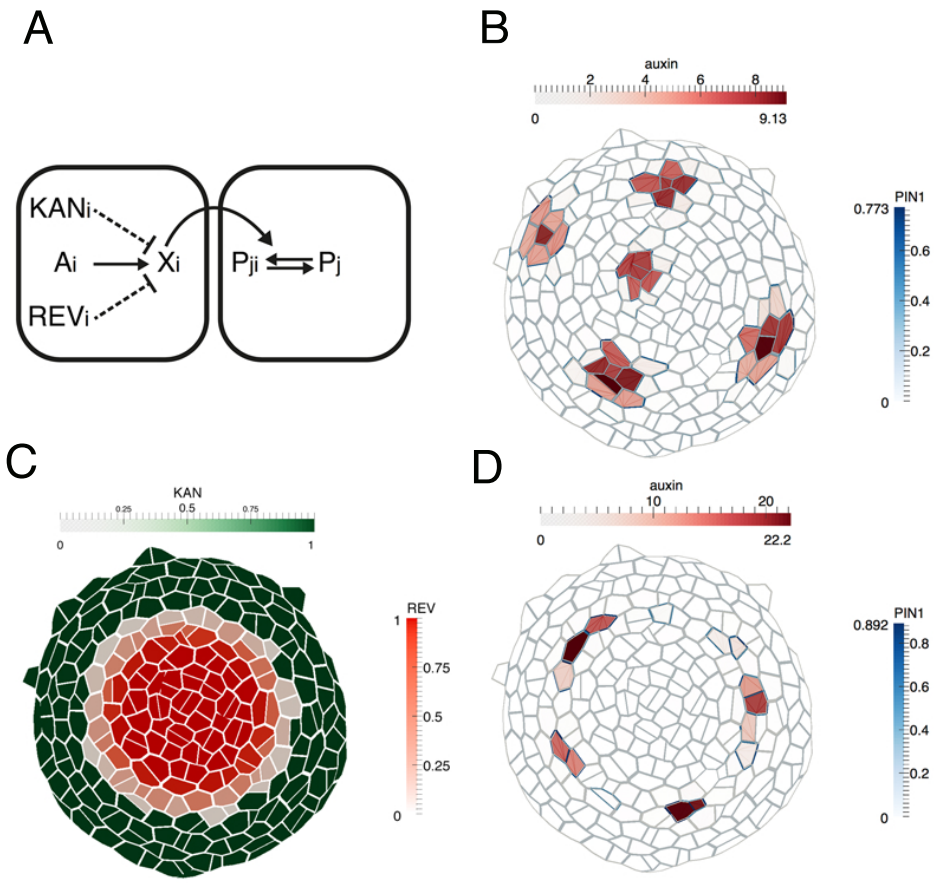

Figure 9.

Computational model illustrating how dorsoventral gene expression boundaries may restrict phyllotactic patterning to the SAM peripheral zone.

(**A**) Illustration of model interactions. Auxin is transported passively and actively via PIN1 between cells. PIN1 is polarized towards cells with high auxin, via a signaling pathway represented by X (previously suggested to be realized by increased stresses in the neighboring cells due to changes in mechanical wall properties (Heisler et al., 2010). (**B**) As shown previously (Heisler et al., 2010; Jonsson et al., 2006; Smith et al., 2006), peaks of auxin are formed spontaneously. (**C**) A pattern of KANADI (green) and REVOLUTA (red) is added to the template with a boundary domain in between in which REV expression is low or absent and KAN1 expression is absent. (**D**) If KANADI and REVOLUTA decrease the signal X in cells where they are expressed (dashed interactions in A), the formation of auxin peaks is restricted to the boundary.

bioRxiv preprint doi: https://doi.org/10.1101/126466; this version posted June 9, 2017. The copyright holder for this preprint (which was not certified by peer review) is the author/funder, who has granted bioRxiv a license to display the preprint in perpetuity. It is made available under aCC-BY 4.0 International license.

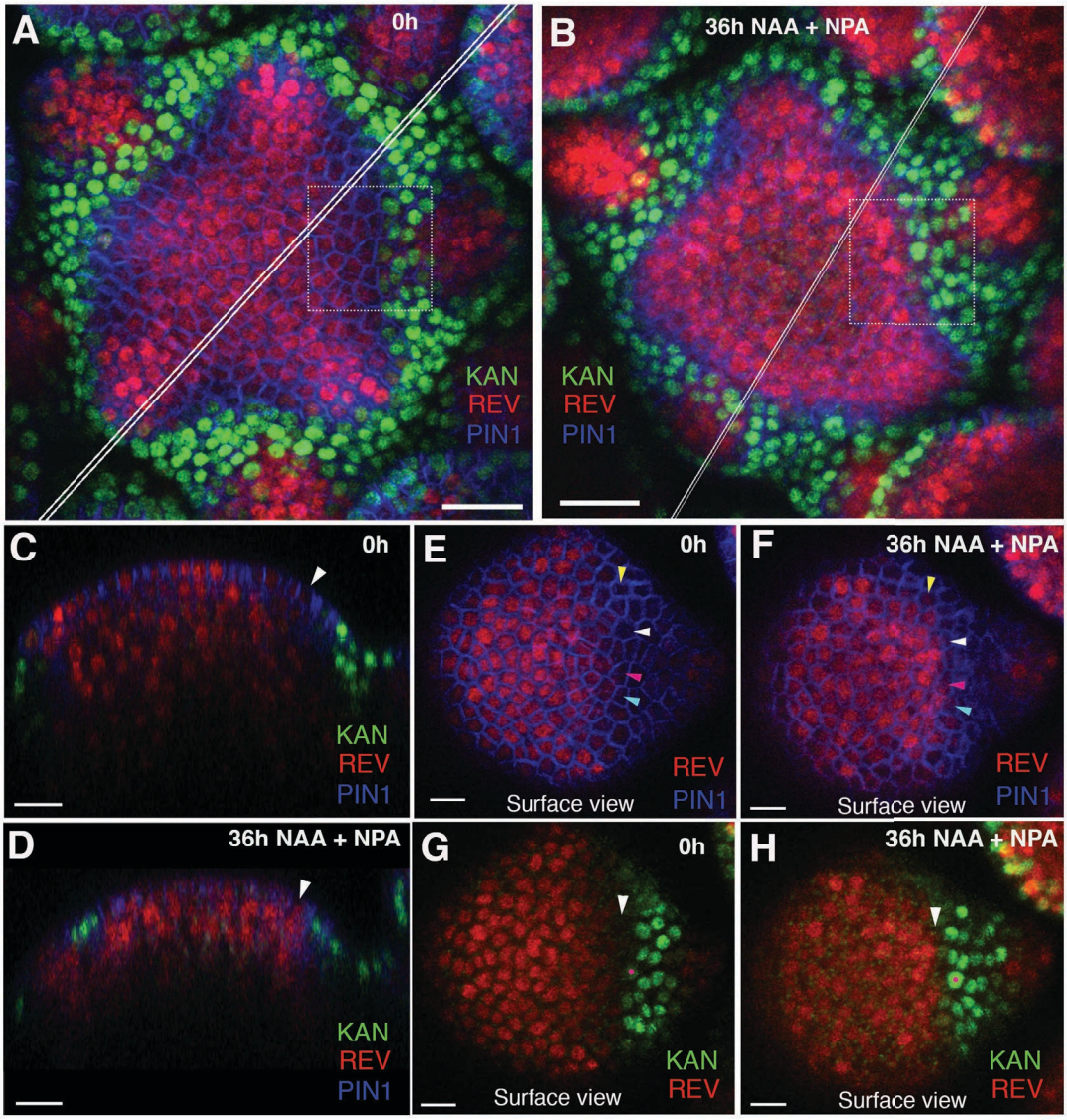

Figure 10- Effect of auxin on the expression patterns of REV and KAN1 in the inflorescence meristem

(A and B) Confocal projections of the IMs showing expression pattern of REV-2×YPet (red), KAN1-2×GFP (green) and PIN1-CFP (blue) before (A) and 36 hours after the combined application of 5mM NAA and 100µM NPA (B). Note REV expression has broadened slightly after the application of NAA and NPA combination (n=2/3). (**C** and **D**) Longitudinal optical sections along the white lines in (A) and (B) respectively. Note the presence of REV in the epidermal cell marked by a white arrowhead in (D) and its absence in (C). (**E** and **F**) Surface views of the regions outlined in dotted rectangles in (A) and (B) respectively, showing PIN1 expression in blue and REV expression in red

bioRxiv preprint doi: https://doi.org/10.1101/126466; this version posted June 9, 2017. The copyright holder for this preprint (which was not certified by peer review) is the author/funder, who has granted bioRxiv a license to display the preprint in perpetuity. It is made available under aCC-BY 4.0 International license.

1100 before (E) and after NAA plus NPA treatment (F). Note the presence of REV expression
1101 in the cells marked by colored arrowheads in (F) and its absence in the same cells prior to
1102 NAA plus NPA application (E). (**G** and **H**) Same as (E and F) but showing REV
1103 expression (red) along with KAN 1 expression (green). Note the presence of a gap (white
1104 arrowhead) between REV and KAN1 expression in (G) but absence (white arrowhead) in
1105 (H). Red dots in (G and H) mark the same cell tracked over 36 hours. Scale bars 20μm (A
1106 and B) and 10μm (C-H).
1107

bioRxiv preprint doi: https://doi.org/10.1101/126466; this version posted June 9, 2017. The copyright holder for this preprint (which was not certified by peer review) is the author/funder, who has granted bioRxiv a license to display the preprint in perpetuity. It is made available under aCC-BY 4.0 International license.

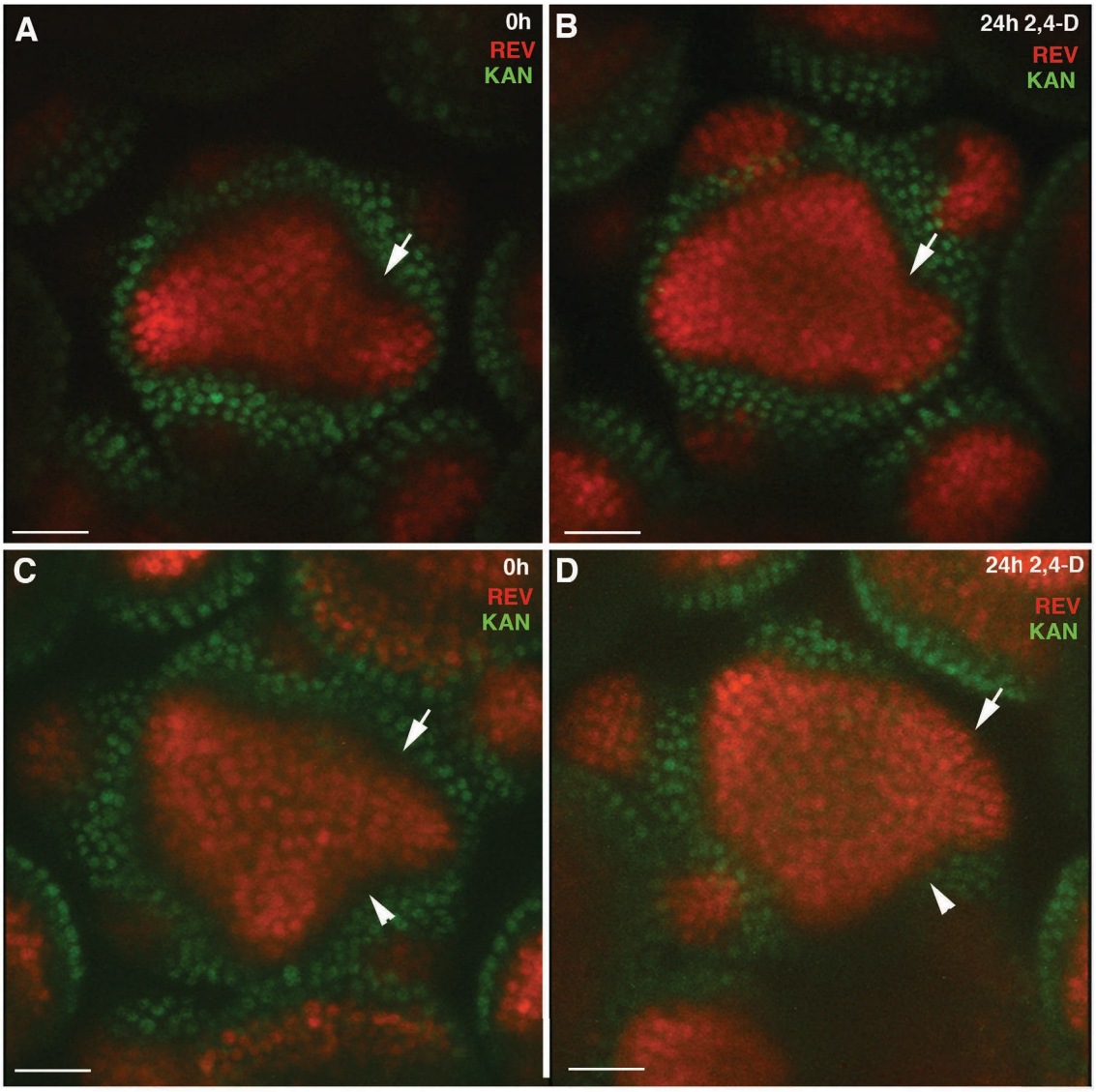

Figure 10 -Figure Supplement 1

Expression of REV in response to exogenous 2,4-D

(A) REV-2xVENUS (red) and KAN1-2xGFP (green) expression in a wild type apex before 2,4-D treatment**.** Expression normally decreases in primordial boundary regions (arrow) **(B)** Inflorescence shown in (A) 24 hours after 2,4-D treatment. Expression in boundary region is maintained (arrow). **(C)** Another inflorescence expressing REV-2xVENUS and KAN1-2xGFP. Note cells in which both REV and KAN1 expression appears absent (arrows). **(D)** Same inflorescence as shown in (C) 24 hours after 2,4-D treatment showing REV expression now extending to the boundary of KAN1 expression

bioRxiv preprint doi: https://doi.org/10.1101/126466; this version posted June 9, 2017. The copyright holder for this preprint (which was not certified by peer review) is the author/funder, who has granted bioRxiv a license to display the preprint in perpetuity. It is made available under aCC-BY 4.0 International license.

1120 (arrows). This REV expression is continuous between new primordial positions

1121 indicating a lack of inter-organ down- regulation. Scale bars, 30μm (A-D)

1122

1123

bioRxiv preprint doi: https://doi.org/10.1101/126466; this version posted June 9, 2017. The copyright holder for this preprint (which was not certified by peer review) is the author/funder, who has granted bioRxiv a license to display the preprint in perpetuity. It is made available under aCC-BY 4.0 International license.

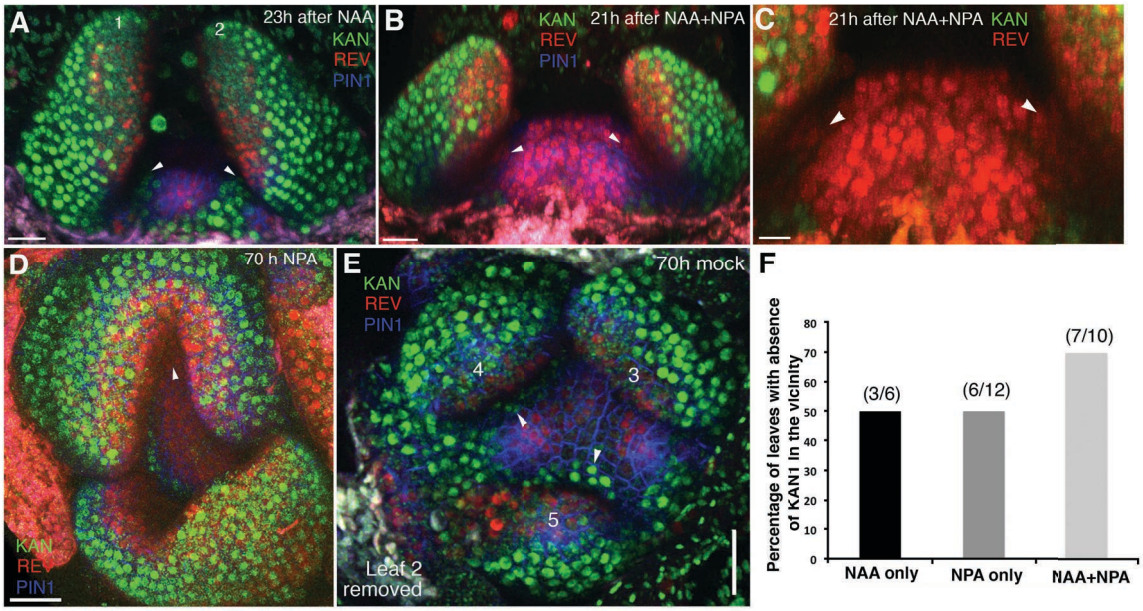

Figure 11. High auxin levels prevent new KAN1 expression in the leaf axils.

(**A-E**) Confocal projection of the VM showing expression pattern of REV-2×YPet (red), KAN1-2×GFP (green) and PIN1-CFP (blue) 23 hours after the treatment with 5mM NAA (A), 21 hours after combined treatment with NAA and NPA (B and C); panel (C) showing close-up view of the meristem in (B) with REV (red) and KAN (green) expression only, 70 hours after treatment with NPA alone (D) and 70 hours after treatment with mock (E). White arrowheads mark the presence of KAN1 expression in the cells adjacent to the grown out leaves in (A) and (E) and absence in (B-D). Note that REV expression (red) expanded towards leaves axils in (B-D). However also note that REV expression appears faint in the leaf axils in (B and C) compared to (D). This is due to the reason that the combined application of NAA and NPA resulted in the leaves growing at an acute angle to the meristem, which caused shading and made it difficult to reach leaf axils while imaging. (**E**) A bar graph showing percentages of leaves lacking KAN1 expression in their vicinity upon treatment with NAA, NPA and NAA+NPA. Scale bars 20μm (A and B), 10μm in (C) and 30μm (D and E).

bioRxiv preprint doi: https://doi.org/10.1101/126466; this version posted June 9, 2017. The copyright holder for this preprint (which was not certified by peer review) is the author/funder, who has granted bioRxiv a license to display the preprint in perpetuity. It is made available under aCC-BY 4.0 International license.

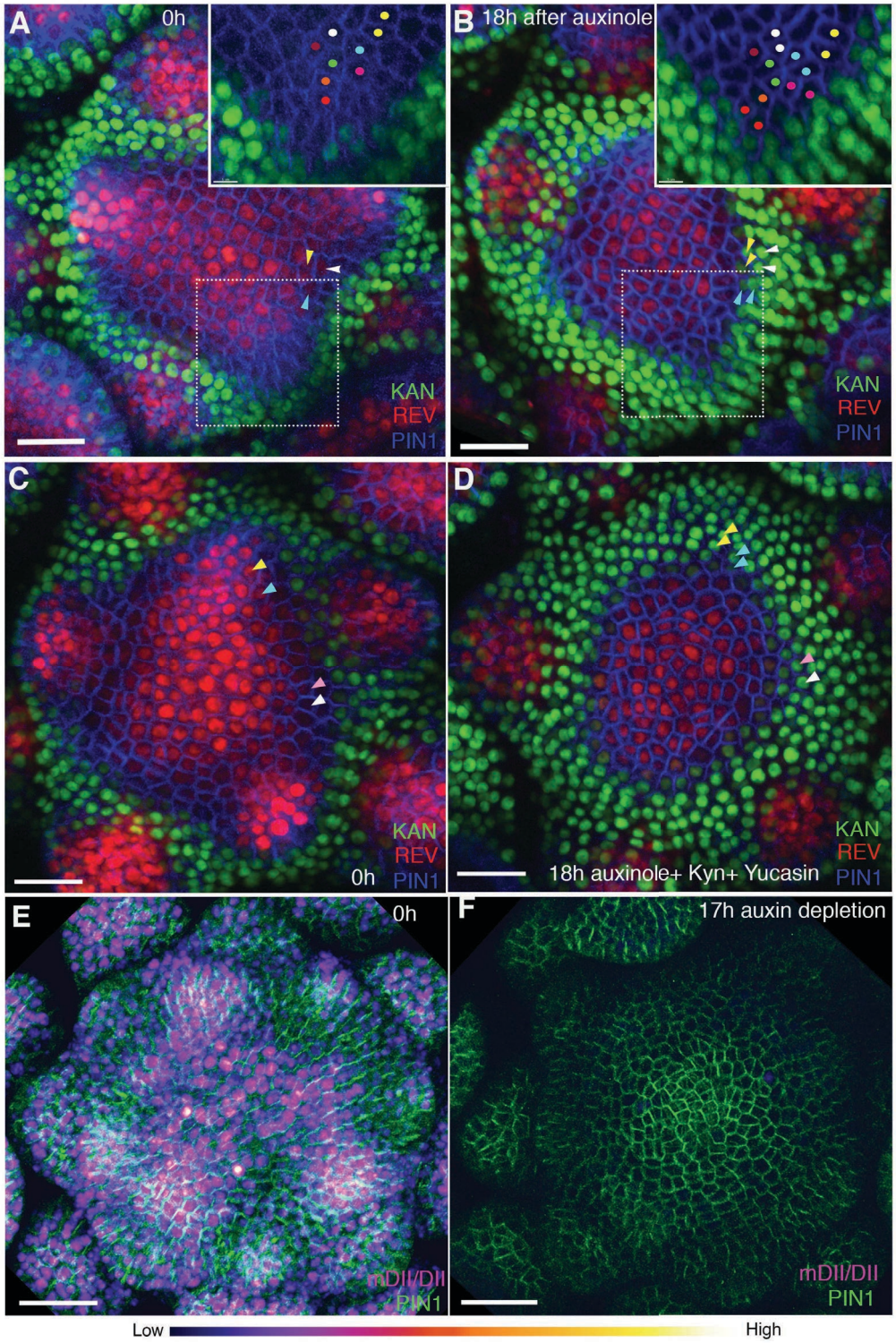

Figure 12 Auxin depletion alters boundary position

(**A** and **B**) Confocal projections of the IMs showing expression pattern of REV-2×YPet (red), KAN1-2×GFP (green) and PIN1-CFP (blue) before (A) and 18 hours (B) after the application of 100μM auxinole. Inset shows close-up of the primordium outlined with the

bioRxiv preprint doi: https://doi.org/10.1101/126466; this version posted June 9, 2017. The copyright holder for this preprint (which was not certified by peer review) is the author/funder, who has granted bioRxiv a license to display the preprint in perpetuity. It is made available under aCC-BY 4.0 International license.

dotted rectangle. Similar colored dots mark the same cells at 0h and 18h time-points. Note the presence of KAN1 expression in the proximity of the cells marked with colored dots in the inset in (A) and its absence in the inset in (B). Similar color arrowheads in (A and B) mark the same cells that showed REV expression at 0h but KAN1 expression at 18h after treatment with auxinole. **(C and D)** Confocal projections of the IMs showing expression pattern of REV-2×YPet (red), KAN1-2×GFP (green) and PIN1-CFP (blue) before (C) and 18 hours (D) after the combined application of 100µM auxinole, 100µM KYN and 100µM Yucasin (auxin depleting drugs). Note KAN-2×GFP expression has expanded centrally at the expense of REV-2×YPet expression (compare the cells marked by arrowheads in (C) with (D), similar colored arrowheads mark the same cells tracked over 18 hours) (n=6/6). (**E** and **F**) Confocal projections of the IMs indicating the predicted auxin distribution (magenta) based on R2D2 expression along with PIN1-GFP expression (green) before (E) and 17 hours after the combined application of 100µM auxinole, 100µM kyn and 100µM yucasin (auxin depleting drugs) (F). Note lack of detectable auxin based on R2D2 expression in (F) compared to (E) after the combined drug application (n=3/4). Scale bars 20µm (A-D), 30µm (E and F).

bioRxiv preprint doi: https://doi.org/10.1101/126466; this version posted June 9, 2017. The copyright holder for this preprint (which was not certified by peer review) is the author/funder, who has granted bioRxiv a license to display the preprint in perpetuity. It is made available under aCC-BY 4.0 International license.

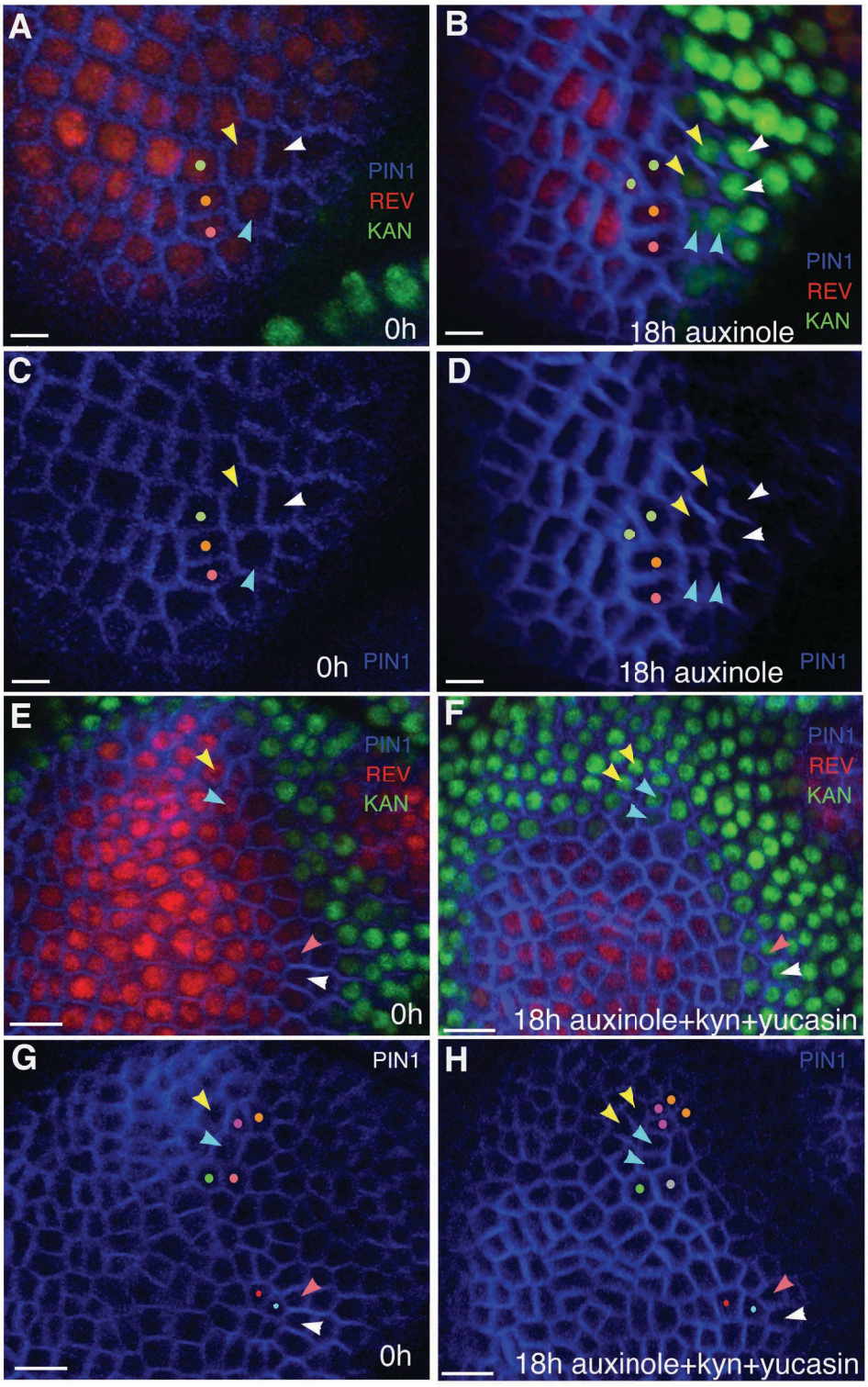

Figure 12-Figure Supplement 1

Auxin depletion results in KAN expression at the expense of REV

bioRxiv preprint doi: https://doi.org/10.1101/126466; this version posted June 9, 2017. The copyright holder for this preprint (which was not certified by peer review) is the author/funder, who has granted bioRxiv a license to display the preprint in perpetuity. It is made available under aCC-BY 4.0 International license.

(**A and B**) Close-up views of cells marked with arrowheads in Figure 12A (A) and Figure 12B (B) showing PIN1 (blue), KAN (green) and REV expression (red). Similar colored arrowheads mark the same cells tracked over 18 hours (same as in Figure 12 (A and B). (**C** and **D**) Same as (A and B) but showing PIN1 expression alone to clearly highlight cell outlines for their identification after 18 hours of treatment with auxinole. (**E and F**) Close-up views of the cells marked with arrowheads in Figure 12C (E) and Figure 12D (F) showing PIN1 (blue), KAN (green) and REV expression (red). Similar colored arrowheads mark the same cells tracked over 18 hours (same as in Figure 12 (C and D). (**G** and **H**) Same as (E and F) but showing PIN1 expression alone to clearly highlight cell outlines for their identification, 18 hours after combined treatment with auxinole, yucasin and kyn. Cells marked with same colored dots are tracked over 18 hours in (A-H). Scale bars, 5μm (A-D) and 10 μm (E-H).

bioRxiv preprint doi: https://doi.org/10.1101/126466; this version posted June 9, 2017. The copyright holder for this preprint (which was not certified by peer review) is the author/funder, who has granted bioRxiv a license to display the preprint in perpetuity. It is made available under aCC-BY 4.0 International license.

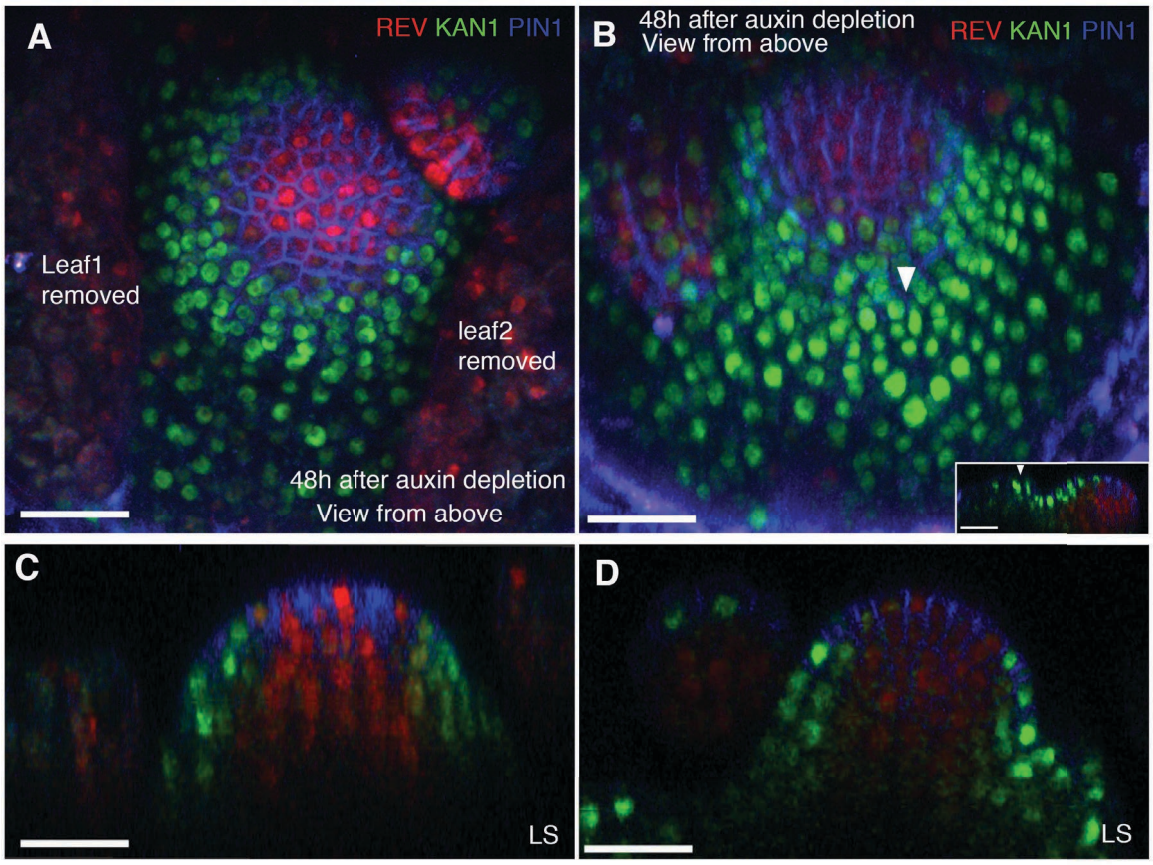

Figure 12-Figure supplement 2

Auxin depletion alters dorsoventral gene expression in the vegetative meristems.

(A and B) Confocal projections of the VMs showing expression pattern of REV-2×YPet (red), KAN1-2×GFP (green) and PIN1-CFP (blue) 48 hours after the combined application of 100µM auxinole, 100µM KYN and 100µM Yucasin (auxin depleting drugs). Arrowhead in (B) marks an arrested leaf primordium expressing KAN throughout. Inset in (B) shows a longitudinal optical section of the leaf primordium ectopically expressing KAN1-2×GFP. **(C and D)** Longitudinal optical sections of the VMs in (A) and (B) respectively. Note that the meristems grow as pins with no new organs initiating. Scale bars 30µm (A-D, inset in B).

bioRxiv preprint doi: https://doi.org/10.1101/126466; this version posted June 9, 2017. The copyright holder for this preprint (which was not certified by peer review) is the author/funder, who has granted bioRxiv a license to display the preprint in perpetuity. It is made available under aCC-BY 4.0 International license.

1199

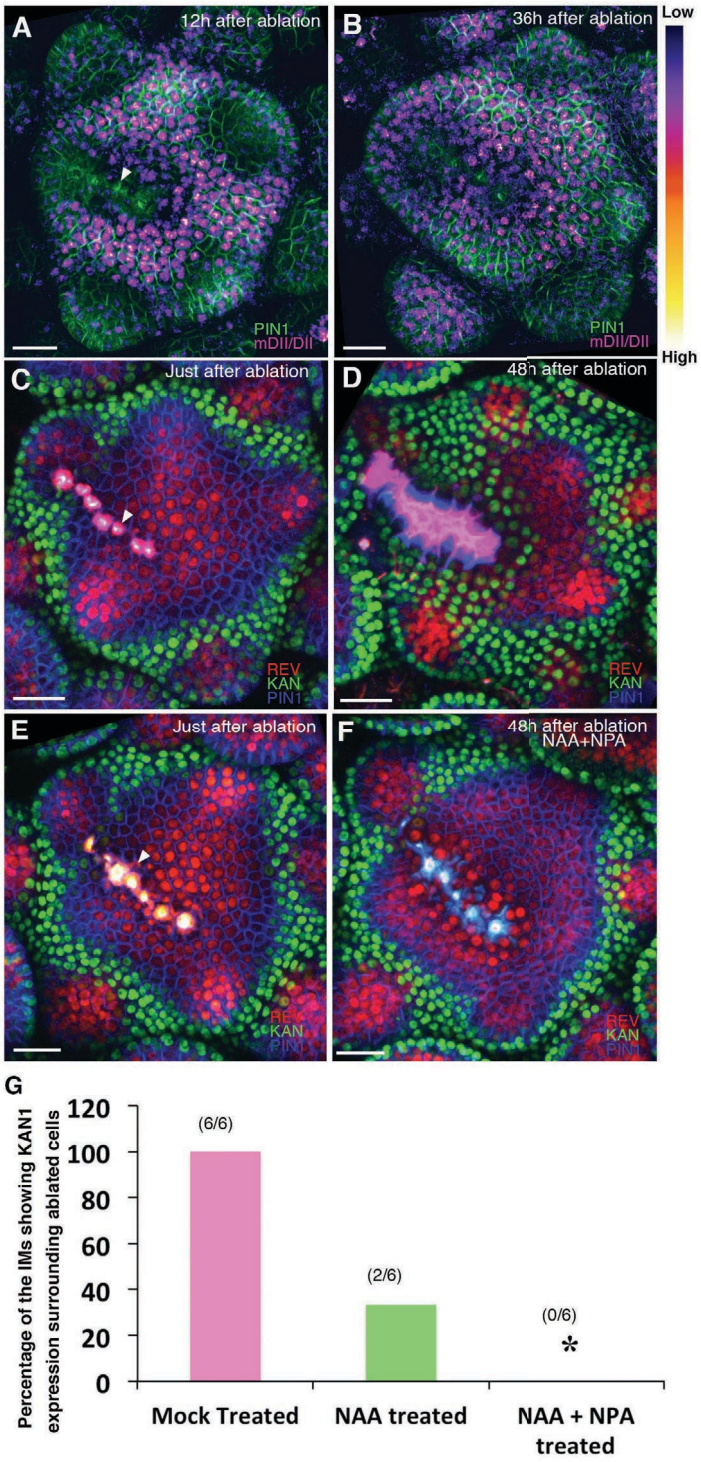

1200

1201 **Figure 13.**

1202 **Wounding induces KANADI1 expression in response to low auxin.**

1203 **(A and B)** Confocal projections of IMs showing predicted auxin distribution (magenta)

1204 based on R2D2 expression 12hours (A) and 36 hours (B) after wounding. Note low

bioRxiv preprint doi: https://doi.org/10.1101/126466; this version posted June 9, 2017. The copyright holder for this preprint (which was not certified by peer review) is the author/funder, who has granted bioRxiv a license to display the preprint in perpetuity. It is made available under aCC-BY 4.0 International license.

predicted auxin levels in the cells surrounding the ablated cells. **(C and D)** Confocal projections of the IMs showing expression pattern of REV-2×YPet (red), KAN1-2×GFP (green) and PIN1-CFP (blue) immediately after ablation (ablated cells indicated a white arrowhead) (C) and 48 hours after (D). Note KAN1 expression (green) has completely surrounded the wounded cells 48h after the ablation (D) compared to (C). **(E and F)** Confocal projections of the IMs showing expression pattern of REV-2×YPet (red), KAN1-2×GFP (green) and PIN1-CFP (blue) immediately after ablation (ablated cells are marked by white arrowhead) (E) and 48 hours after ablation and combined NAA and NPA application (F). Note absence of KAN1 expression (green) surrounding the wound when wounding is accompanied by the exogenous addition of auxin and NPA (compare to (D)). (**G**) Quantification of wounding induced ectopic KAN1 expression upon mock treatment (n=6/6)), NAA application (n=2/6)) and NAA + NPA combination (n= 0/6) application on the Arabidopsis IMs expressing REV-2×YPet, KAN1-2×GFP and PIN1-CFP. Scale bars 30μm (A-F).

bioRxiv preprint doi: https://doi.org/10.1101/126466; this version posted June 9, 2017. The copyright holder for this preprint (which was not certified by peer review) is the author/funder, who has granted bioRxiv a license to display the preprint in perpetuity. It is made available under aCC-BY 4.0 International license.

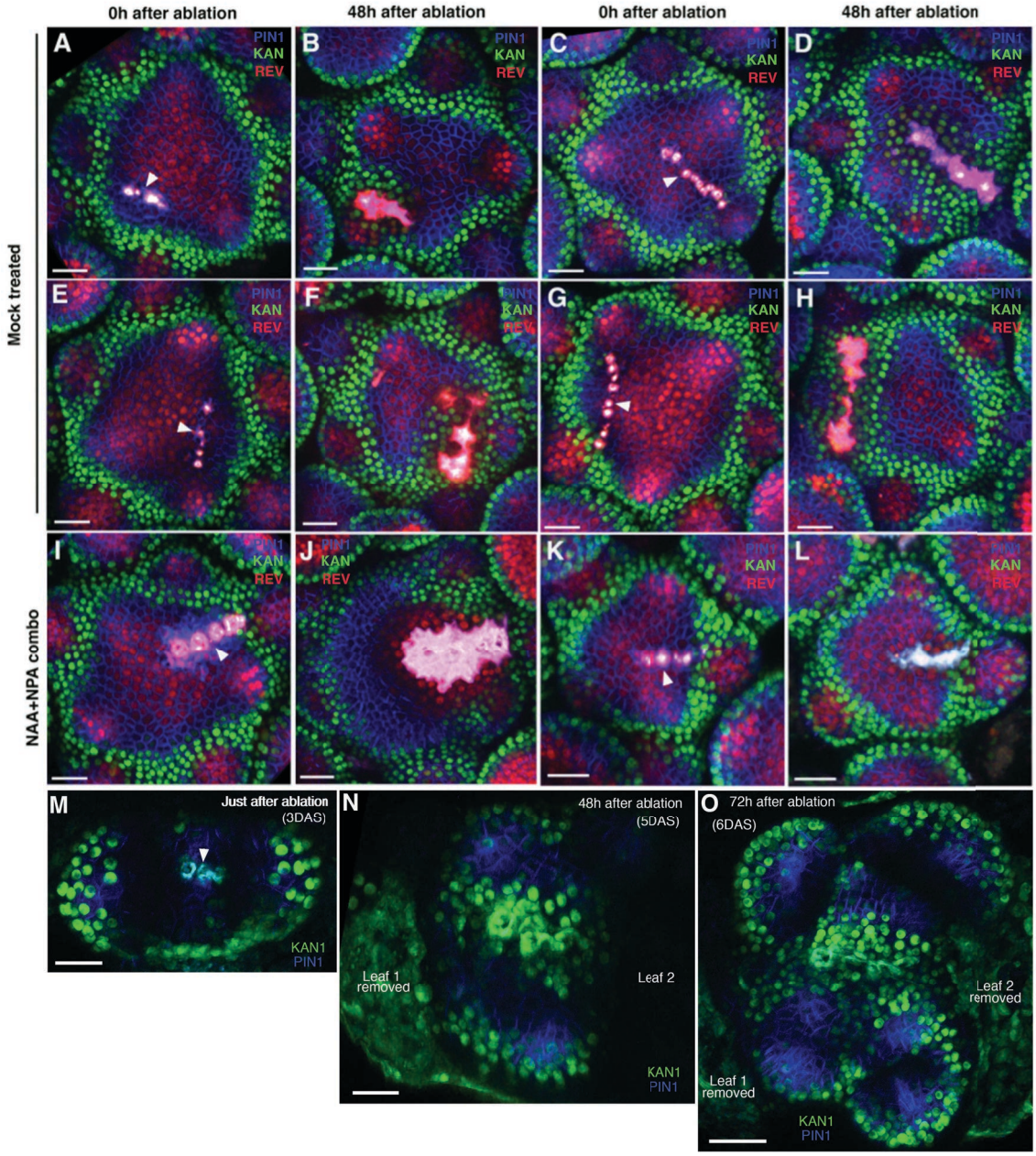

Figure 13-Figure Supplement 1

Wounding induces ectopic KAN expression in the inflorescence and vegetative meristems.

(**A-H**) Confocal projections of the inflorescence meristems showing expression pattern of KAN1-2×GFP (green) and PIN1-CFP (blue) immediately after ablation (A, C, E, and G) and corresponding meristems 48 hours after ablation (B, D, F and H). Note ectopic KAN1 expression on both the sides of the ablated cells 48 hours after wounding. (**I-L**) Confocal projections of inflorescence meristems showing expression pattern of KAN1-

bioRxiv preprint doi: https://doi.org/10.1101/126466; this version posted June 9, 2017. The copyright holder for this preprint (which was not certified by peer review) is the author/funder, who has granted bioRxiv a license to display the preprint in perpetuity. It is made available under aCC-BY 4.0 International license.

2×GFP (green) and PIN1-CFP (blue) immediately after (I and K) and 48 hours after ablation and treatment with NAA and NPA (J and L). Note lack of ectopic KAN1 expression compared to comparable untreated meristems (B, D, F and H). (**M-O**) Confocal projections of the vegetative meristems showing expression pattern of KAN1-2×YPet (green) and PIN1-GFP (blue) immediately after ablation (M), 48 hours after ablation (N) and 72hours after ablation (O). Ablated cells are marked by arrowhead in (M). 72 hours after wounding the vegetative meristem appears split into at least two distinct meristems with new leaves oriented normally with respect to each meristem (O). Scale bars 20µm (A to N); 30µm (O).

bioRxiv preprint doi: https://doi.org/10.1101/126466; this version posted June 9, 2017. The copyright holder for this preprint (which was not certified by peer review) is the author/funder, who has granted bioRxiv a license to display the preprint in perpetuity. It is made available under aCC-BY 4.0 International license.

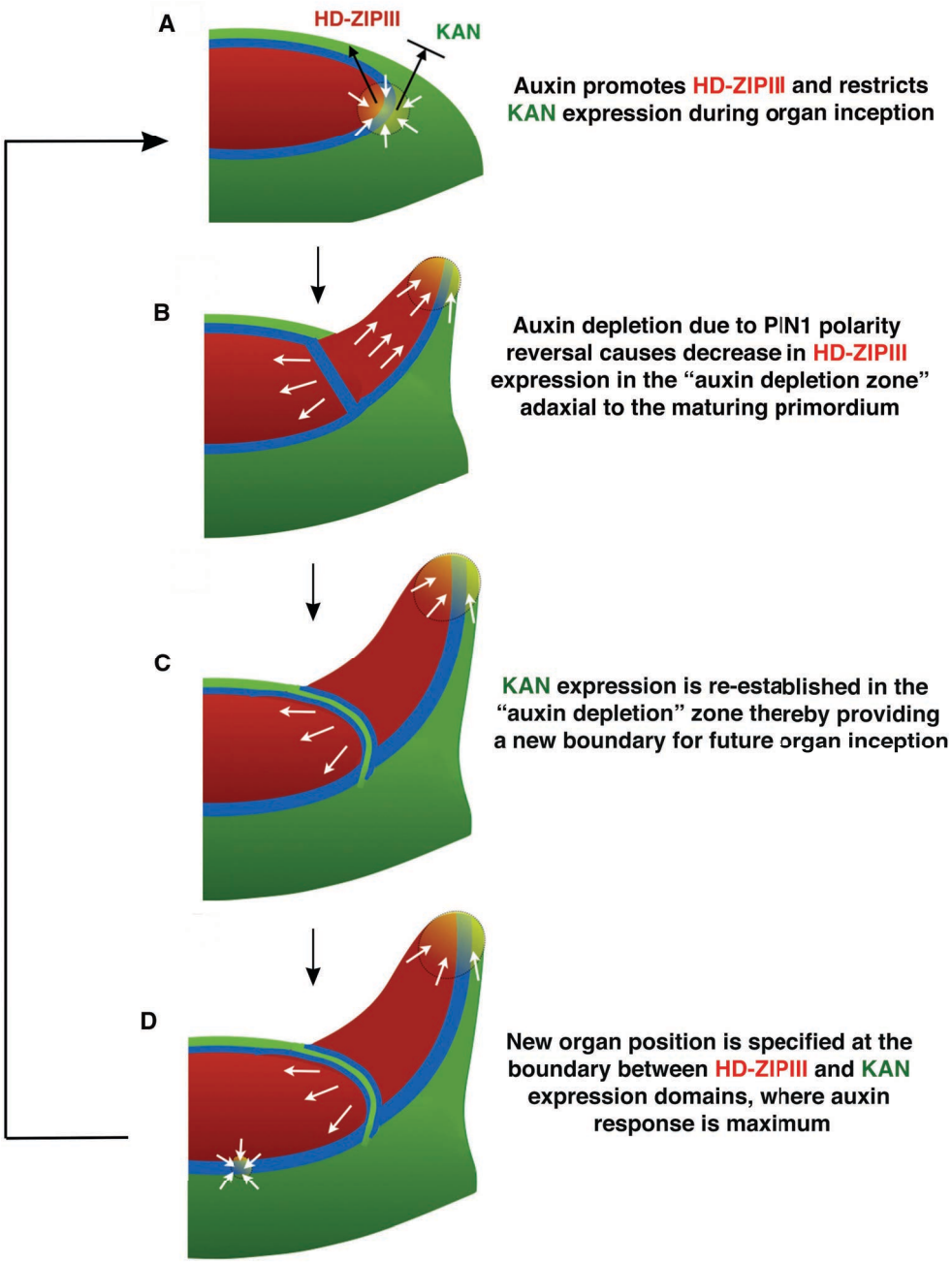

Figure 14: Conceptual Model.

(**A**) During organ inception, PIN1 polarities (white arrows) and the alignment of microtubule arrays converge to create an auxin maximum and promote growth oriented towards the epidermal boundary between HD-ZIPIII and KANADI (KAN) expression domains. As auxin accumulates, it promotes the expression of HD-ZIPIII thereby resulting in its extension towards the PIN1 convergence site. At the same time, auxin also

bioRxiv preprint doi: https://doi.org/10.1101/126466; this version posted June 9, 2017. The copyright holder for this preprint (which was not certified by peer review) is the author/funder, who has granted bioRxiv a license to display the preprint in perpetuity. It is made available under aCC-BY 4.0 International license.

prevents the expansion of KAN adaxially. Thus the boundary becomes fixed to the underlying cells. (**B**) As the primordium grows, PIN1 polarity in cells adaxial to the primordium reverse towards the meristem center and adjacent incipient primordia, thereby creating an auxin depletion zone leading to a reduction in HD-ZIPIII expression. (**C**) The reduction in auxin results in the re-establishment of KAN expression between the meristem and organ. (**D**) Auxin in the vicinity of the boundary in adjacent tissues leads to a localized transcriptional response that orients the polarity of surrounding cells into a convergence pattern, most likely via mechanical signals (Bhatia et al., 2016).

bioRxiv preprint doi: https://doi.org/10.1101/126466; this version posted June 9, 2017. The copyright holder for this preprint (which was not certified by peer review) is the author/funder, who has granted bioRxiv a license to display the preprint in perpetuity. It is made available under aCC-BY 4.0 International license.

Movie S1

Movie shows confocal 3D projection of a single vegetative seedling corresponding to that shown in Fig. 6, G and H. Several leaf-like organs have formed on the boundary of ectopic KAN1 expression driven by the CLV3 promoter (green). These organs express REV (red) in restricted patterns corresponding to the three classes described in Fig. 6 (labeled Class 2, 3 and 4). Note developing leaf margins, marked by high PIN1 expression (blue) correlate with REV expression boundaries in the epidermis.

Movie S2

Confocal projection of an Arabidopsis seedling 70 hours after treatment with NPA showing view of the vegetative meristem from above with channels for PIN1-CFP (blue), REV-2x YPet (red) and KAN1-2xGFP (green) alternating (also shown as a snapshot in Figure 11C). Note the absence of contiguous KAN1 expression in between the meristem and older leaves potentially due to auxin build up in the absence of its regular transport.

Computational model files (separate file as one zipped archive)

Archive containing files used for the computational model. Files will be extracted to the directory modelFiles, and further information is found in the file README.txt in this directory.